VERSITA
Int. J. of Applied Mechanics and Engineering, 2013, vol.18, No.4, pp.1115-1150
DOI: 10.2478/ijame-2013-0070

EFFECT OF CHEMICAL REACTION AND RADIATION ON DOUBLE DIFFUSIVE FLOW OF A VISCOUS, DISSIPATIVE FLUID THROUGH POROUS MEDIUM IN A RECTANGULAR CAVITY WITH HEAT SOURCES

T.L. RAJU and P. MURALIDHAR*
Dept. of Engineering Mathematics
A.U. College of Engineering (A), Andhra University
Visakhapatnam-530 003, A.P., INDIA
E-mail: tlraju45@yahoo.com; muralidhar.pmd@gmail.com

In this paper, an attempt is made to discuss the combined influence of radiation and dissipation on the convective heat and mass transfer flow of a viscous fluid through a porous medium in a rectangular cavity using the Darcy model. Making use of the incompressibility, the governing non-linear coupled equations for the momentum, energy and diffusion are derived in terms of the non-dimensional stream function, temperature and concentration. The Galerkin finite element analysis with linear triangular elements is used to obtain the global stiffness matrices for the values of stream function, temperature and concentration. These coupled matrices are solved using an iterative procedure and expressions for the stream function, temperature and concentration are obtained as linear combinations of the shape functions. The behavior of temperature, concentration, the Nusselt number and Sherwood number is discussed computationally for different values of the governing parameters, such as the Rayleigh Number (Ra), heat source parameter (α), Eckert number (Ec), Schmidt Number (Sc), Soret parameter (S_0), buoyancy ratio (N).

Key words: heat and mass transfer flow, radiation, dissipation, heat sources, rectangular cavity, porous medium.

1. Introduction

The study of heat transfer and mixed convection flow in porous medium enclosures of various shapes has received much attention. Interest in these natural convection flows and heat transfer in a porous medium has been motivated by a broad range of applications, including geothermal systems, crude oil production, storage of nuclear waste materials, ground water pollution, fiber and granular insulations, solidification of castings, etc. In a wide range of such problems, the physical system can be modeled as a two-dimensional rectangular enclosure with vertical walls held at different temperatures and the connecting horizontal walls considered adiabatic. Convective heat transfer in a rectangular porous duct, whose vertical walls are maintained at two different temperatures and horizontal walls insulated, is a problem which has received attention of many investigators. Some of these works include numerical results.

The investigation of heat transfer in enclosures containing porous media began with the experimental work of Verschoor and Greebler (1952). Verschoor and Greebler (1952) were followed by several other investigators interested in porous media heat transfer in rectangular enclosures. In particular, Bankvall (1972; 1973; 1974) published a great deal of practical work concerning heat transfer by natural convection in rectangular enclosures completely filled with porous media. Burns *et al*. (1926) described a porous medium heat transfer flow in a rectangular geometry. Cheng and Hi (1987) studied the flow and heat transfer rate in a rectangular box with solid walls using a Brinkman model, when the box is differentially heated in the horizontal direction. Chen *et al*. (1970) considered enclosures with the aspect ratio greater than or equal to

* To whom correspondence should be addressed

one. Their numerical computations indicate that when the Darcy number based on the width of the enclosures is less than 10^{-9}, Darcy's law and the Brinkman equation virtually give the same results for the heat transfer rate. Joseph *et al.* (1964) considered laminar forced convection in rectangular channels with unequal heat addition on adjacent sides. Teomann Ayhan *et al.* (1998) considered heat transfer and flow structure in a rectangular channel with wing-type vortex generator. Han-Chieh Chiu *et al.* (2007) discussed mixed convection heat transfer in horizontal rectangular ducts with radiation effects. Chittibabu *et al.* (2006) discussed convective flow in a porous rectangular duct with differentially heated side walls using a Brinkman model.

When heat and mass transfer occur simultaneously, it leads to a complex fluid motion called double-diffusive convection. Double-diffusion occurs in a wide range of scientific fields such as oceanography, astrophysics, geology, biology and chemical processes. Viskanta *et al.* (1985) published complete reviews on the subject. Bejan (1979) wrote a fundamental study of scale analysis relative to heat and mass transfer within cavities submitted to horizontal combined and pure temperature and concentration gradients. Kamotani *et al.* (1985) conducted experiments on mass transfer and flow pattern in shallow enclosures (*H\L=0*, *13-0.55*) filled with a fluid (P_r = *7*, Sc = *2100*) in cases where the combined buoyancy effect is dominated by the buoyancy due to the concentration gradient. Other experimental studies dealing with thermo solute convection in rectangular enclosures were reported by Lee *et al.* (1990). Lee and Hyun (1985; 1990), Hyun and Lee (1990) reported numerical solutions for unsteady double-diffusive convection in a rectangular enclosure with aiding and opposing temperature and concentration gradients that were in good agreement with reported experimental results. The most recent review of this activity is the one published by Viskanta *et al.* (1985), where it is stressed that the two requirements for the occurrence of double-diffusive convection are that the fluid contains two or more components with different molecular diffusivities and that these components make opposing contributions to the vertical density gradients. Trevisan and Bejan (1987) analyzed natural convection in a rectangular enclosure with uniform heat and mass fluxes along the vertical sides analytically and numerically. He obtained Oseen linearised solution for all spaces filled with mixtures characterized by Le = *1* and arbitrary buoyancy ratios.

The effect of varying the Lewis number (Le) is documented by a similarity solution valid for Le > *1* in heat transfer driven flows and for Le < *1* mass transfer driven flows. Mass line patterns are used to visualize the convective mass transfer rate and the flow reversal is observed when the buoyancy ratio *n = 1*. Also Trevisan *et al.* (1987) studied natural convection heat and mass transfer through a vertical porous layer subjected to uniform fluxes of heat and mass from the side. The Oseen linearised solution that yielded the overall heat and mass transfer correlation was developed for a porous medium and a buoyancy effect ruled by both temperature and concentration variations in the high Rayleigh number region where the heat and mass transfer rates differ greatly from estimates based on the assumption of pure diffusion. The similarity solution that produced the overall mass transfer was developed for different parametric domains.

The effect of viscous dissipation on heat transfer has been studied for different geometries. Beckermann (1987) studied the viscous dissipation effect on natural convection in a horizontal cylinder embedded in a porous medium. Their study showed that the viscous dissipation affect the natural convection in a porous cavity and found that the heat transfer rate at hot surface decreases with increase of viscous dissipation parameter. Thermal radiation plays a significant role in the overall surface heat transfer where convective heat transfer is small. Verschoor *et al.* (1952) studied the effect of viscous dissipation and radiation on an unsteady magnetohydrodynamic free convection flow past a vertical plate in a porous medium. They found that the temperature profile increases when viscous dissipation increases. A good amount of work has been done to understand natural convection in a porous cavity. In spite of many efforts to study heat transfer in a porous cavity, the combined effect of viscous dissipation and radiation on a porous medium filled inside a square cavity has not received much attention in the literature. Badruddin *et al.* (2006) investigated the radiation and viscous dissipation on convective heat transfer in a porous cavity. Recently Padmavathi (2009) analyzed the connective heat transfer through a porous medium in a rectangular cavity with heat sources and dissipation under varied conditions. Ranga Reddy (1997) discussed the natural convective heat and mass transfer in a porous rectangular cavity with differentially heated side walls using the Brinkman model by solving the governing equations with the Galerkin finite element analysis. Sivaiah *et*

al. (2004) investigated the double-diffusive convective heat transfer flow of a viscous fluid through a porous medium with a rectangular duct with thermo-diffusion effect by using the finite element technique. Reddaiah *et al.* (2010) analyzed the effect of viscous dissipation on convective heat and mass transfer flow of a viscous fluid in a duct of a rectangular cross section by employing the Galerkin finite element analysis.

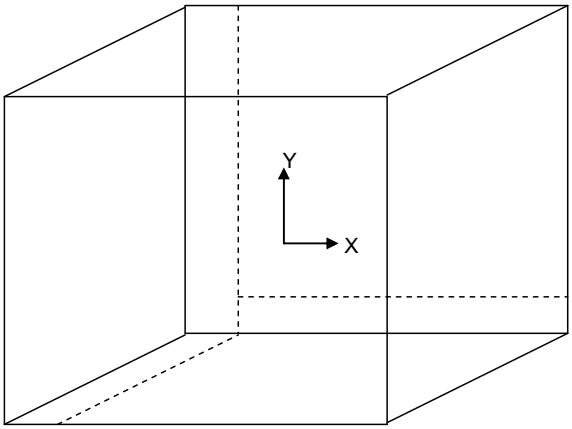

Fig.I. Schematic diagram of the flow model.

2. Formulation of the problem

We consider the mixed convective heat and mass transfer flow of a viscous incompressible fluid in a saturated porous medium confined in the rectangular duct (Fig.I) whose base length is "a", height "b". The heat flux on the base and top walls is maintained constant. The Cartesian coordinate system O (x, y) is chosen with the origin on the central axis of the duct and its base parallel to the x-axis. We assume that

i) The convective fluid and the porous medium are everywhere in local thermodynamic equilibrium.
ii) There is no phase change of the fluid in the medium.
iii) The properties of the fluid and of the porous medium are homogeneous and isotropic.
iv) The porous medium is assumed to be closely packed so that Darcy's momentum law is adequate in the porous medium.
v) The Boussinesq approximation is applicable.

Under these assumption the governing equations are given by

$$\frac{\partial u'}{\partial x'}+\frac{\partial v'}{\partial y'}=0\,, \tag{2.1}$$

$$u'=-\frac{k}{\mu}\left(\frac{\partial p'}{\partial x'}\right), \tag{2.2}$$

$$v'=-\frac{k}{\mu}\left(\frac{\partial p'}{\partial y'}+\rho' g\right), \tag{2.3}$$

$$\rho_\sigma c_p\left(u'\frac{\partial T'}{\partial x'}+v'\frac{\partial T'}{\partial y'}\right)=K_1\left(\frac{\partial^2 T'}{\partial x'^2}+\frac{\partial^2 T'}{\partial y'^2}\right)+Q\left(T_0-T\right)+\left(\frac{\mu}{k}\right)\left(u^2+v^2\right)-\frac{\partial(q_r)}{\partial x}, \tag{2.4}$$

$$\rho_\sigma c_p \left(u' \frac{\partial C}{\partial x'} + v' \frac{\partial C}{\partial y'} \right) = D_1 \left(\frac{\partial^2 C}{\partial x'^2} + \frac{\partial^2 C}{\partial y'^2} \right) + k_{11} \left(\frac{\partial^2 T}{\partial x'^2} + \frac{\partial^2 T}{\partial y'^2} \right) - KC, \tag{2.5}$$

$$\rho' = \rho_0 \left\{ 1 - \beta \left(T' - T_0 \right) - \beta^{\bullet} \left(C' - C_0 \right) \right\}, \tag{2.6}$$

$$T_0 = \frac{T_h + T_c}{2}, \qquad C_0 = \frac{C_h + C_c}{2}$$

where, u' and v' are Darcy velocities along the x- and y- directions, respectively. T', C, p' and g' are the temperature; concentration, pressure and acceleration due to gravity. T_c, C_c, T_h and C_h are the temperature and concentration on the cold and warm side walls, respectively. ρ', μ, ν and β are the density, coefficients of viscosity, kinematic viscosity and thermal expansion of the fluid, k is the permeability of the porous medium, K_1 is the thermal conductivity, C_p is the specific heat at constant pressure, Q is the strength of the heat source, k_{11} is the cross diffusivity, β^* is the volume coefficient of expansion with mass fraction concentration, k is the concentration coefficient and q_r is the radiative heat flux. The boundary conditions are

$$\begin{aligned}
&u' = v' = 0 && \text{on the boundary of the duct} \\
&T' = T_c, \quad C = C_c && \text{on the side wall to the left} \\
&T' = T_h, \quad C = C_h && \text{on the side wall to the right} \\
&\frac{\partial T'}{\partial y} = 0, \quad \frac{\partial C}{\partial y} = 0 && \text{on the top } (y = 0) \text{ and bottom} \\
&u = v = 0 && \text{walls } (y = 0) \text{ which are insulated.}
\end{aligned} \tag{2.7}$$

Invoking Rosseland approximation for radiation

$$q_r = \frac{4\sigma^*}{3\beta_R} \frac{\partial T'^4}{\partial y}.$$

Expanding T^4 in Taylor's series about T_e and neglecting higher order terms

$$T'^4 \cong 4T_e^3 T - 3T_e^4.$$

We now introduce the following non-dimensional variables

$$\begin{aligned}
&x' = ax; \qquad y' = by \quad ; \qquad h = b/a, \\
&u' = (\nu/a)\, u; \quad v' = (\nu/a)\, v; \quad p' = (\nu^2 \rho/a^2)\, p, \\
&T' = T_0 + \theta\, (T_h - T_c), \qquad C' = C_0 + C\, (T_h - T_c).
\end{aligned} \tag{2.8}$$

The governing equations in the non-dimensional form are

$$u = -\left(\frac{k}{a^2}\right)\frac{\partial p}{\partial x}, \tag{2.9}$$

$$v = -\frac{k}{a^2}\frac{\partial p}{\partial y} - \frac{kag}{v^2} + \frac{kag\beta\left(T_h - T_c\right)\theta}{v^2} + \frac{kag\beta^{\bullet}\left(C_h - C_c\right)C}{v^2}, \tag{2.10}$$

$$P\left(u\frac{\partial\theta}{\partial x} + v\frac{\partial\theta}{\partial y}\right) = \left(1 + \frac{4N}{3}\right)\left(\frac{\partial^2\theta}{\partial x^2} + \frac{\partial^2\theta}{\partial y^2}\right) - \alpha\theta + E_C\left(u^2 + v^2\right), \tag{2.11}$$

$$\mathrm{Sc}\left(u\frac{\partial C}{\partial x} + v\frac{\partial C}{\partial y}\right) = \left(\frac{\partial^2 C}{\partial x^2} + \frac{\partial^2 C}{\partial y^2}\right) + \frac{\mathrm{ScSo}}{N}\left(\frac{\partial^2\theta}{\partial x^2} + \frac{\partial^2\theta}{\partial y^2}\right) - k_1 C, \tag{2.12}$$

In view of the equation of continuity, we introduce the stream function ψ as

$$u = \frac{\partial\psi}{\partial y}; \qquad v = -\frac{\partial\psi}{\partial x}. \tag{2.13}$$

Eliminating *p* from Eqs (2.9) and (2.10) and making use of Eq.(2.11) the equations in terms of ψ and θ are

$$\nabla^2\psi - M_1^2\frac{\partial^2\psi}{\partial x^2} = -\mathrm{Ra}\left(\frac{\partial\theta}{\partial x} + N\frac{\partial C}{\partial x}\right), \tag{2.14}$$

$$P\left(\frac{\partial\psi}{\partial y}\frac{\partial\theta}{\partial x} - \frac{\partial\psi}{\partial x}\frac{\partial\theta}{\partial y}\right) = \left(1 + \frac{4}{3N_1}\right)\left(\frac{\partial^2\theta}{\partial x^2} + \frac{\partial^2\theta}{\partial y^2}\right) - \alpha\theta + \mathrm{E_C}\left(\left(\frac{\partial\psi}{\partial y}\right)^2 + \left(\frac{\partial\psi}{\partial x}\right)^2\right), \tag{2.15}$$

$$\mathrm{Sc}\left(\frac{\partial\psi}{\partial y}\frac{\partial C}{\partial x} - \frac{\partial\psi}{\partial x}\frac{\partial C}{\partial y}\right) = \left(\frac{\partial^2 C}{\partial x^2} + \frac{\partial^2 C}{\partial y^2}\right) + \frac{\mathrm{ScSo}}{N}\left(\frac{\partial^2\theta}{\partial x^2} + \frac{\partial^2\theta}{\partial y^2}\right) - \gamma C \tag{2.16}$$

where

$G = \dfrac{g\beta\left(T_h - T_c\right)a^3}{v^2}$ (Grashof number), $\quad \mathrm{P} = \mu\, c_p/K_1$ (Prandtl number)

$\alpha = Qa^2/K_1$ (heat source parameter), $\quad \mathrm{Ra} = \dfrac{\beta g\left(T_g - T_c\right)Ka}{\nu^2}$ (Rayleigh number)

$N_1 = \dfrac{3\beta_R K_1}{4\sigma^{\bullet}:T_e^3}$ (radiation parameter), $\quad \mathrm{Sc} = \dfrac{\nu}{D}$ (Schmidt number)

$\mathrm{So} = \dfrac{k_{11}\beta^{\bullet}}{\nu\beta}$ (Soret parameter), $\quad N = \dfrac{\beta^*\left(C_h - C_c\right)}{\beta\left(T_h - T_c\right)}$ (buoyancy ratio)

$\mathrm{Ec} = \left(\dfrac{a^4}{\mu K K_1 \Delta T}\right)$ (Eckert number), $\quad \gamma = \dfrac{k_1 L^2}{D_1}$ (chemical reaction parameter).

The boundary conditions are

$$\frac{\partial \psi}{\partial x} = 0, \qquad \frac{\partial \psi}{\partial y} = 0 \qquad \text{on} \qquad x = 0, \qquad \text{and} \qquad 1, \tag{2.17}$$

$$\theta = 1, \qquad c = 1 \qquad \text{on} \qquad x = 0,$$

$$\theta = 0, \qquad c = 0 \qquad \text{on} \qquad x = 1. \tag{2.18}$$

3. Finite element analysis and solution of the problem

The region is divided into a finite number of three node triangular elements, in each of which the element equation is derived using the Galerkin weighted residual method. In each element e_i, f_i is an approximate solution for an unknown f in the variational formulation and can be expressed as a linear combination of shape function, $\left(N_k^i\right)\ k = 1,2,3,$ which are linear polynomials in x and y. This approximate solution of the unknown f coincides with actual values at each node of the element. The variational formulation results in a *3 x 3* matrix equation (stiffness matrix) for the unknown local nodal values of the given element. These stiffness matrices are assembled in terms of global nodal values using inter element continuity and boundary conditions resulting in a global matrix equation.

In each case, there are r distinct global nodes in the finite element domain and f_p ($p = 1, 2, \ldots\ldots r$) are the global nodal values of any unknown f defined over the domain. Then $f = \sum_{i=1}^{8} \sum_{p=1}^{r} f_p \ \Phi_p^i$, where the first summation denotes summation over s elements and the second one represents summation over the independent global nodes and $\Phi_p^i = N_N^i,$ if p is one of the local nodes, say k of the element $e_i = 0$, otherwise. f_p's are determined from the global matrix equation. Based on these lines, we now make a finite element analysis of the given problem governed by Eqs (2.14)-(2.16) subjected to the conditions (2.17)-(2.18).

Let ψ^i, θ^i and C^i be the approximate values of ψ, θ and C in an element θ_i.

$$\psi^i = N_1^i \ \psi_1^i \ + N_2^i \ \psi_2^i + \ N_3^i \ \psi_3^i, \tag{3.1a}$$

$$\theta^i = N_1^i \ \theta_1^i \ + N_2^i \ \theta_2^i + \ N_3^i \ \theta_3^i, \tag{3.1b}$$

$$C = N_1^i \ C_1^i \ + N_2^i \ C_2^i + \ N_3^i \ C_3^i. \tag{3.1c}$$

Substituting the approximate value ψ^i, θ^i and C^i for ψ, θ and C, respectively, in Eq.(2.13) the error is as follows

$$E_1^i = \left(1 + \frac{4}{3N_1}\right)\frac{\partial^2 \theta^i}{\partial x^2} + \frac{\partial^2 \theta^i}{\partial y^2} - P\left(\frac{\partial \psi^i}{\partial y} \ \frac{\partial \theta^i}{\partial x} \ - \frac{\partial \psi^i}{\partial x} \ \frac{\partial \theta^i}{\partial y}\right) + \\ -\alpha\theta + \mathrm{Ec}\left[\left(\frac{\partial \psi}{\partial y}\right)^2 + \left(\frac{\partial \psi}{\partial x}\right)^2\right], \tag{3.2}$$

$$E_2^i = \frac{\partial^2 C^i}{\partial x^2} + \frac{\partial^2 C^i}{\partial y^2} - \mathrm{Sc}\left(\frac{\partial \psi^i}{\partial y} \ \frac{\partial C^i}{\partial x} \ - \frac{\partial \psi^i}{\partial x} \ \frac{\partial C^i}{\partial y}\right) + \frac{\mathrm{ScSo}}{N}\left(\frac{\partial^2 C^i}{\partial x^2} + \frac{\partial^2 C^i}{\partial y^2}\right) - \gamma C. \tag{3.3}$$

Under the Galerkin method this error is made orthogonal over the domain of e_i to the respective shape functions (weight functions) where

$$\int_{ei} E_1^i N_k^i d\Omega = 0\,,$$

$$\int_{ei} E_2^i N_k^i d\Omega = 0,$$

$$\int_{ei} N_k^i \left(1+\frac{4}{3N_1}\right)\left(\frac{\partial^z \theta^i}{\partial x^2}+\frac{\partial^z \theta^i}{\partial y^2}\right) - P\left(\frac{\partial \psi^i}{\partial y}\ \frac{\partial \theta^i}{\partial x}\ -\frac{\partial \psi^i}{\partial x}\ \frac{\partial \theta^i}{\partial y}\right)+$$
$$-\alpha\theta+\left[\mathrm{Ec}\left(\frac{\partial \psi}{\partial y}\right)^2+\left(\frac{\partial \psi}{\partial x}\right)^2\right]d\Omega = 0, \tag{3.4}$$

$$\int_{ei} N_k^i \left(\left(\frac{\partial^z C^i}{\partial x^2}+\frac{\partial^z C^i}{\partial y^2}\right)-\mathrm{Sc}\left(\frac{\partial \psi^i}{\partial y}\ \frac{\partial C^i}{\partial x}\ -\frac{\partial \psi^i}{\partial x}\ \frac{\partial C^i}{\partial y}\right)+\right.$$
$$\left.+\frac{\mathrm{ScSo}}{N}\left(\frac{\partial^z \theta^i}{\partial x^2}+\frac{\partial^z \theta^i}{\partial y^2}\right)-\gamma C\right)d\Omega = 0. \tag{3.5}$$

Using Green's theorem we reduce the surface integral Eqs (3.4) and (3.5) without affecting ψ terms and obtain

$$\int_{ei} N_k^i \left\{\left(1+\frac{4}{3N_1}\right)\frac{\partial N_k^i}{\partial x}\ \frac{\partial \theta^i}{\partial x}+\frac{\partial N_k^i}{\partial y}\ \frac{\partial \theta^i}{\partial y}-P_1 N_k\left(\frac{\partial \psi^i}{\partial y}\ \frac{\partial \theta^i}{\partial x}\ -\frac{\partial \psi^i}{\partial x}\ \frac{\partial \theta^i}{\partial y}\right)+\right.$$
$$\left.-\alpha\theta\ +\ \mathrm{Ec}\left(\frac{\partial \psi}{\partial y}\right)^2+\left(\frac{\partial \psi}{\partial x}\right)^2 d\Omega\right\} = \int_{\Gamma i} N_k^i\left(\frac{\partial \theta^i}{\partial x}n_x+\frac{\partial \theta^i}{\partial y}n_y\right)d\Gamma_i\,, \tag{3.6}$$

$$\int_{eiei} N_k^i \left\{\frac{\partial N_k^i}{\partial x}\ \frac{\partial C^i}{\partial x}+\frac{\partial N_k^i}{\partial y}\ \frac{\partial C^i}{\partial y}-\mathrm{Sc}^i N_k\left(\frac{\partial \psi^i}{\partial y}\ \frac{\partial C^i}{\partial x}\ -\frac{\partial \psi^i}{\partial x}\ \frac{\partial C^i}{\partial y}\right)+\right.$$
$$\left.+\frac{\mathrm{ScSo}^2}{N}\left(\frac{\partial N_k^i}{\partial x}\ \frac{\partial \theta^i}{\partial x}+\frac{\partial N_k^i}{\partial y}\ \frac{\partial \theta^i}{\partial y}\right)-\gamma C\right\}d\Omega = \int_{\Gamma i} N_k^i\left(\frac{\partial \theta^i}{\partial x}+\frac{\mathrm{ScSo}}{N}\frac{\partial C^i}{\partial x}\right)n_x + \tag{3.7}$$
$$+\left(\frac{\partial \theta^i}{\partial y}+\frac{\mathrm{ScSo}}{N}\frac{\partial C^i}{\partial y}n_y\right)d\Gamma_i$$

where, Γ_1 is the boundary of e_i.

Substituting L.H.S. of Eqs (3.1a) - (3.1c) for ψ^i, θ^i and C^i in Eqs (3.6) and (3.7), we get

$$\sum_1 \int_{ei}\left(1+\frac{4N}{3}\right)\frac{\partial N_k^i}{\partial x}\ \frac{\partial N_L^i}{\partial x}+\frac{\partial N_L^i}{\partial y}\ \frac{\partial N_k^i}{\partial y}+$$
$$-P\sum_1 \psi_m^i \int_{ei}\left(\frac{\partial N_m^i}{\partial y}\ \frac{\partial N_L^i}{\partial x}-\frac{\partial N_m^i}{\partial x}\ \frac{\partial N_L^i}{\partial y}\right)d\Omega-\alpha\sum\theta^i\int_{ei} N\,N_{k\,l}\,d\Omega_i+$$
$$+\mathrm{Ec}\int_{ei}\left(\left(\frac{\partial \psi}{\partial y}\right)^2+\left(\frac{\partial \psi}{\partial x}\right)^2\right)d\Omega = \int_{\Gamma_i} N_k^i\left(\frac{\partial \theta^i}{\partial x}\ n_x+\frac{\partial \theta^i}{\partial y}n_y\right)d\Gamma_i = Q_k^i,\left(l,\ m,\ k=1,2,3\right), \tag{3.8}$$

$$\sum_{l}\int_{ei} C^i\left(\frac{\partial N_k^i}{\partial x}\ \frac{\partial N_L^i}{\partial x}+\frac{\partial N_L^i}{\partial y}\ \frac{\partial N_k^i}{\partial y}\right)-\mathrm{Sc}\sum_{l}\psi_m^i\int_{ei}\left(\frac{\partial N_m^i}{\partial y}\ \frac{\partial N_L^i}{\partial x}-\frac{\partial N_m^i}{\partial x}\ \frac{\partial N_L^i}{\partial y}\right)d\Omega+$$
$$+\frac{\mathrm{ScSo}}{N}\sum\theta^i\int_{ei}\left(\frac{\partial N_k^i}{\partial x}\ \frac{\partial N_L^i}{\partial x}+\frac{\partial N_L^i}{\partial y}\ \frac{\partial N_k^i}{\partial y}\right)-\gamma\int_{e_i} C^i d\Omega^i{}_i = \tag{3.9}$$
$$=\int_{\Gamma i} N_k^i\left(\frac{\partial\theta^i}{\partial x}+\frac{\mathrm{ScSo}}{N}\frac{\partial\theta^i}{\partial x}\right)n_x+\left(\frac{\partial\theta^i}{\partial y}+\frac{\mathrm{ScSo}}{N}\frac{\partial\theta^i}{\partial y}n_y\right)d\Gamma_i=Q_i^C,$$
$$(l,\ m,\ k=1,\ 2,\ 3)$$

where, $Q_k^i=Q_{k1}^i+Q_{k2}^i+Q_{k3}^i, Q_k^i$'s being the values of Q_k^i on the sides s = (*1*, *2*, *3*) of the element e_i. The sign of Q_k^i 's depends on the direction of the outward normal with respect to the element. Choosing different N_k^i 's as weight functions and following the same procedure we obtain matrix equations for three unknowns (Q_p^i), viz.

$$\left(a_p^i\right)\left(\theta_p^i\right)=\left(Q_k^i\right) \tag{3.10}$$

where, $\left(a_{pk}^i\right)$ is a *3* x *3* matrix, $\left(\theta_p^i\right),\left(Q_k^i\right)$ are column matrices. Repeating the above process with each of *s* elements, we obtain sets of such matrix equations. Introducing the global coordinates and global values for θ_p^i and making use of inter element continuity and boundary conditions relevant to the problem the above stiffness matrices are assembled to obtain a global matrix equation. This global matrix is *r* x *r* square matrix if there are *r* distinct global nodes in the domain of the flow considered.

Similarly, substituting ψ^i, θ^i and ϕ^i in Eq.(2.12) and defining the error

$$E_3^i=\nabla^2\psi-M^2\psi+\mathrm{Ra}\left(\frac{\partial\theta}{\partial x}+N\frac{\partial C}{\partial x}\right), \tag{3.11}$$

and following the Galerkin method we obtain

$$\int_{\Omega} E_3^i\psi^i{}_j d\Omega=0. \tag{3.12}$$

Using Green's theorem (3.8) reduces to

$$\int_{\Omega}\left(\frac{\partial N_k^i}{\partial x}\ \frac{\partial\psi^i}{\partial x}+\frac{\partial N_k^i}{\partial y}\ \frac{\partial\psi^i}{\partial y}+\mathrm{Ra}\left(\theta^i\frac{\partial N_k^i}{\partial x}+C^i\frac{\partial N_k^i}{\partial x}\right)\right)d\Omega=$$
$$=\int_{\Gamma}N_k^i\left(\frac{\partial\psi^i}{\partial x}\ n_x+\frac{\partial\psi^i}{\partial y}n_y\right)d\Gamma_i\ +\int_{\Gamma}N_k^i n_x\theta^i d\Gamma_i. \tag{3.13}$$

In obtaining (3.13) Green's theorem is applied with respect to derivatives of ψ without affecting θ terms.

Using Eqs (3.1) and (3.2) in Eq.(3.13) we have

$$\sum_m \psi_m^i \left\{ \int_\Omega \left(\frac{\partial N_k^i}{\partial x} \frac{\partial N_m^i}{\partial x} + \frac{\partial N_m^i}{\partial y} \frac{\partial N_k^i}{\partial y} \right) d\Omega_i + \right.$$

$$\left. + \mathrm{Ra} \sum_L \theta_L^i \int_{\Omega^i} N_k^i \frac{\partial N_L^i}{\partial x} d\Omega + C_L^i N \int_{\Omega^i} N_k^i \frac{\partial N_L^i}{\partial x} d\Omega \right\} = \tag{3.14}$$

$$= \int_\Gamma N_k^i \left(\frac{\partial \psi^i}{\partial x} n_x + \frac{\partial \psi^i}{\partial y} n_y \right) d\Gamma_i + \int_\Gamma N_k^i \theta^i d\Omega_i = \Gamma_k^i .$$

In the problem under consideration, for computational purposes, we choose a uniform mesh of 10 triangular elements (Fig.II). The domain has vertices whose global coordinates are (*0*, *0*), (*1*, *0*) and (*1*, *c*) in the non-dimensional form. Let e_1, e_2…..e_{10} be the ten elements and let θ_1, θ_2, … θ_{10} be the global values of θ and ψ_1, ψ_2,…,ψ_{10} be the global values of ψ at the ten global nodes of the domain (Fig.II).

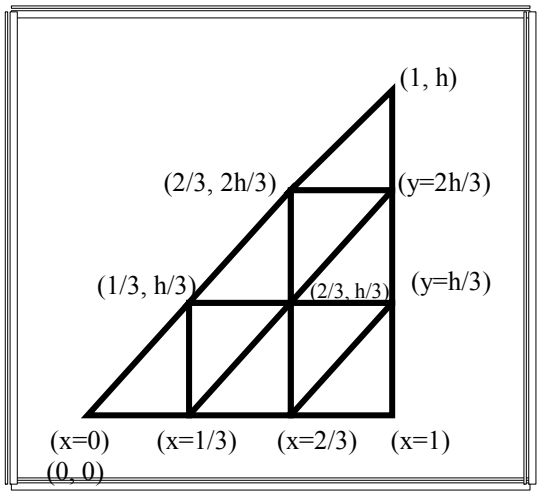

Fig.II. Schematic diagram of the configuration.

4. Shape of functions and stiffness of matrices

Range functions in $n_{i,j}$; i = element, j = node.

$$n_{1,1} = 1 - 3x, \quad n_{1,2} = 3x - \frac{3y}{h}, \quad n_{2,1} = 1 - \frac{3y}{h}, \quad n_{2,2} = -1 + \frac{3y}{h},$$

$$n_{2,3} = 1 - 3x + \frac{3y}{h}, \quad n_{3,1} = 2 - 3x, \quad n_{3,2} = -1 + 3x - \frac{3y}{h}, \quad n_{3,3} = \frac{3y}{h},$$

$$n_{4,1} = 1 - \frac{3y}{h}, \quad n_{4,2} = -2 + 3x, \quad n_{4,3} = 2 - 3x + \frac{3y}{h}, \quad n_{5,1} = 2 - 3x,$$

$$n_{5,2} = -1 + 3x - \frac{3y}{h}, \quad n_{5,3} = \frac{3y}{h}, \quad n_{6,1} = 2 - 3x, \quad n_{6,2} = 3x - \frac{3y}{h},$$

$$n_{6,3} = 1 + \frac{3y}{h}, \quad n_{7,1} = 2 - \frac{3y}{h}, \quad n_{7,2} = -2 + 3x, \quad n_{7,3} = 1 - 3x + \frac{3y}{h},$$

$$n_{8,1} = 3 - 3x, \quad n_{8,2} = -1 + 3x - \frac{3y}{h}, \quad n_{9,2} = 3x - \frac{3y}{h}, \quad n_{9,3} = -1 + \frac{3y}{h}.$$

Substituting the above shape functions in Eqs (3.8), (3.9) and (3.14) with respect to each element and integrating over the respective triangular domain we obtain the element in the form Eq.(3.8). The *3*x*3* matrix equations are assembled using connectivity conditions to obtain *8*x*8* matrix equations for the global nodes ψ_p, θ_p and C_p.

The global matrix equation for θ is

$$A_3 X_3 = B_3 . \tag{4.1}$$

The global matrix equation for *C* is

$$A_4 X_4 = B_4 . \tag{4.2}$$

The global matrix equation for ψ is

$$A_5 X_5 = B_5 \tag{4.3}$$

where,

$$A_3 = \begin{bmatrix} -1 & a_{12} & a_{13} & 0 & 0 & 0 & 0 & 0 & 0 & 0 & 0 \\ 0 & a_{22} & a_{23} & 0 & 0 & 0 & 0 & 0 & 0 & 0 & 0 \\ 0 & a_{32} & a_{33} & a_{34} & a_{35} & 0 & 0 & 0 & 0 & 0 & 0 \\ 0 & 0 & a_{43} & a_{44} & a_{45} & 0 & 0 & 0 & 0 & 0 & 0 \\ 0 & 0 & a_{53} & a_{54} & a_{55} & a_{56} & a_{57} & 0 & 0 & 0 & 0 \\ 0 & 0 & 0 & 0 & a_{65} & a_{66} & a_{67} & 0 & 0 & 0 & 0 \\ 0 & 0 & 0 & 0 & a_{75} & a_{76} & a_{77} & a_{78} & a_{79} & 0 & 0 \\ 0 & 0 & 0 & 0 & 0 & 0 & a_{87} & a_{88} & a_{89} & 0 & 0 \\ 0 & 0 & 0 & 0 & 0 & 0 & a_{97} & a_{98} & a_{99} & a_{910} & 0 \\ 0 & 0 & 0 & 0 & 0 & 0 & 0 & 0 & a_{109} & a_{1010} & 0 \\ 0 & 0 & 0 & 0 & 0 & 0 & 0 & 0 & a_{119} & a_{1110} & -1 \end{bmatrix},$$

$$A_4 = \begin{bmatrix} 1 & b_{1,2} & b_{1,3} & 0 & 0 & 0 & 0 & 0 & 0 & 0 & 0 \\ 0 & b_{2,2} & b_{2,3} & 0 & 0 & 0 & 0 & 0 & 0 & 0 & 0 \\ 0 & b_{3,2} & b_{3,3} & b_{3,4} & b_{3,5} & 0 & 0 & 0 & 0 & 0 & 0 \\ 0 & 0 & b_{4,3} & b_{4,4} & b_{4,5} & 0 & 0 & 0 & 0 & 0 & 0 \\ 0 & 0 & b_{5,3} & b_{5,4} & b_{5,5} & b_{5,6} & b_{5,7} & 0 & 0 & 0 & 0 \\ 0 & 0 & 0 & 0 & b_{6,5} & b_{6,6} & b_{6,7} & 0 & 0 & 0 & 0 \\ 0 & 0 & 0 & 0 & b_{7,5} & b_{7,6} & b_{7,7} & b_{7,8} & b_{7,9} & 0 & 0 \\ 0 & 0 & 0 & 0 & 0 & 0 & b_{8,7} & b_{8,8} & b_{8,9} & 0 & 0 \\ 0 & 0 & 0 & 0 & 0 & 0 & b_{9,7} & b_{9,8} & b_{9,9} & b_{9,10} & 0 \\ 0 & 0 & 0 & 0 & 0 & 0 & 0 & 0 & b_{10,9} & b_{10,10} & 0 \\ 0 & 0 & 0 & 0 & 0 & 0 & 0 & 0 & b_{11,9} & b_{11,10} & b_{11,11} \end{bmatrix},$$

$$A_5 = \begin{bmatrix} -1 & 0 & 0 & 0 & 0 & 0 & 0 & 0 & 0 & 0 \\ 0 & -1 & 0 & 0 & 0 & 0 & 0 & 0 & 0 & 0 \\ 0 & 0 & -1 & 0 & 0 & 0 & 0 & 0 & 0 & 0 \\ 0 & 0 & 0 & -1 & 0 & 0 & 0 & 0 & 0 & 0 \\ 0 & 0 & 0 & 0 & -1 & 0 & 0 & 0 & 0 & 0 \\ 0 & 0 & 0 & 0 & 0 & 0 & 0 & 0 & 0 & 0 \\ 0 & 0 & 0 & 0 & 0 & 0 & 0 & 0 & 0 & 0 \\ 0 & 0 & 0 & 0 & 0 & 0 & 0 & 0 & 0 & 0 \\ 0 & 0 & 0 & 0 & 0 & 0 & 0 & 0 & -1 & 0 \\ 0 & 0 & 0 & 0 & 0 & 0 & 0 & 0 & 0 & -1 \end{bmatrix},$$

$$X_3 = \begin{bmatrix} \theta_1 \\ \theta_2 \\ \theta_3 \\ \theta_4 \\ \theta_5 \\ \theta_6 \\ \theta_7 \\ \theta_8 \\ \theta_9 \\ \theta_{10} \\ \theta_{11} \end{bmatrix}, \qquad X_4 = \begin{bmatrix} C_1 \\ C_2 \\ C_3 \\ C_4 \\ C_5 \\ C_6 \\ C_7 \\ C_8 \\ C_9 \\ C_{10} \\ C_{11} \end{bmatrix}, \qquad X_5 = \begin{bmatrix} u_1 \\ u_2 \\ u_3 \\ u_4 \\ u_5 \\ u_6 \\ u_7 \\ u_8 \\ u_9 \\ u_{10} \\ u_{11} \end{bmatrix},$$

$$B_3 = \begin{bmatrix} ar_1 \\ ar_2 \\ ar_3 \\ ar_4 \\ ar_5 \\ ar_6 \\ ar_7 \\ ar_8 \\ ar_9 \\ ar_{10} \\ ar_{11} \end{bmatrix}, \qquad B_4 = \begin{bmatrix} br_1 \\ br_2 \\ br_3 \\ br_4 \\ br_5 \\ br_6 \\ br_7 \\ br_8 \\ br_9 \\ br_{10} \\ br_{11} \end{bmatrix}, \qquad B_5 = \begin{bmatrix} cr_1 \\ cr_2 \\ cr_3 \\ cr_4 \\ cr_5 \\ cr_6 \\ cr_7 \\ cr_8 \\ cr_9 \\ cr_{10} \\ cr_{11} \end{bmatrix}.$$

The global matrix equations are coupled and are solved under the following iterative procedures. At the beginning of the first iteration the values of (ψ_i) are taken to be zero and the global Eqs (4.1) and (4.2) are solved for the nodal values of θ and C. These nodal values (θ_i) and (C_i) obtained are then used to solve the global Eq.(4.3) to obtain (ψ_i). In the second iteration these (ψ_i) values are obtained and used in Eqs (4.1) and (4.2) to calculate (θ_i) and (C_i) and vice versa. The three equations are thus solved under the iteration process until two consecutive iterations differ by a reassigned percentage.

The domain consists of three horizontal levels and the solution for Ψ and θ at each level may be expressed in terms of the nodal values as follows,

In the horizontal strip $0 \le y \le \frac{h}{3}$

$$\Psi = \left(\Psi_1 N_1^1 + \Psi_2 N_2^1 + \Psi_7 N_7^1\right) H\ (1-\tau_1),$$

$$= \Psi_1(1-4x) + \Psi_2 4\left(x - \frac{y}{c}\right) + \Psi_7 \frac{4y}{h}(1-\tau_1) \qquad \left(0 \le x \le \frac{1}{3}\right),$$

$$\Psi = \left(\Psi_2 N^3{}_2 + \Psi_3 N^3{}_3 + \Psi_6 N^3{}_6\right) H\ (1-\tau_2) +$$

$$+\left(\Psi_2 N_2^2 + \Psi_7 N_7^2 + \Psi_6 N_6^2\right) H(1-\tau_3) \qquad \left(\frac{1}{3} \le x \le \frac{1}{3}\right),$$

$$= \left(\Psi_2 2(1-2x) + \Psi_3\left(4x - \frac{4y}{h} - 1\right) + \Psi_6\left(\frac{4y}{h}\right)\right) H(1-\tau_2) +$$

$$+\left(\Psi_2\left(1 - \frac{4y}{h}\right) + \Psi_7\left(1 + \frac{4y}{h} - 4x\right) + \Psi_6(4x-1)\right) H(1-\tau_3),$$

$$\Psi = \left(\Psi_3 N_3^5 + \Psi_4 N_4^5 + \Psi_5 N_5^5\right) H\ (1-\tau_3),$$

$$+\left(\Psi_3 N_3^4 + \Psi_5 N_5^4 + \Psi_6 N_6^4\right) H(1-\tau_4) \qquad \left(\frac{2}{3} \le x \le 1\right),$$

$$= \left(\Psi_3(3-4x) + \Psi_4 2\left(2x - \frac{2y}{h} - 1\right) + \Psi_6\left(\frac{4y}{h} - 4x + 3\right)\right) H(1-\tau_3) +$$

$$+\Psi_3\left(1 - \frac{4y}{h}\right) + \Psi_5(4x-3) + \Psi_6\left(\frac{4y}{h}\right)\Big) H\ (1-\tau_4).$$

Along the strip $\frac{h}{3} \le y \le \frac{2h}{3}$

$$\Psi = \left(\Psi_7 N_7^6 + \Psi_6 N_6^6 + \Psi_8 N_8^6\right) H\ (1-\tau_2) + \left(\Psi_6 N_6^7 + \Psi_9 N_9^7 + \Psi_8 N_8^7\right) H(1-\tau_3)$$

$$+\left(\Psi_6 N_6^8 + \Psi_5 N_5^8 + \Psi_9 N_9^8\right) H(1-\tau_4), \qquad \left(\frac{1}{3} \le x \le 1\right),$$

$$\Psi = \left(\Psi_7 2(1-2x) + \Psi_6 (4x-3) + \Psi_8 \left(\frac{4y}{h} - 1 \right) \right) H\ (1-\tau_3) +$$
$$+\Psi_6 \left(2\left(1 - \frac{2y}{h} \right) + \Psi_9 \left(\frac{4y}{h} - 1 \right) + \Psi_8 \left(1 + \frac{4y}{h} - 4x \right) \right) H(1-\tau_4) +$$
$$+ \Psi_6 \left(4(1-x) + \Psi_5 \left(4x - \frac{4y}{h} - 1 \right) + \Psi_9 2 \left(\frac{2y}{h} - 1 \right) \right) H\ (1-\tau_5).$$

Along the strip $\frac{2h}{3} \le y \le 1$

$$\Psi = \left(\Psi_8 N_8^9 + \Psi_9 N_9^9 + \Psi_{10} N_{10}^9 \right) H(1-\tau_6) =$$
$$= \Psi_8 \left(4(1-x) + \Psi_9 4\left(x - \frac{y}{h} \right) + \Psi_{10} 2\left(\frac{4y}{h} - 3 \right) \right) H(1-\tau_6) \qquad \left(\frac{2}{3} \le x \le 1 \right),$$

where $\tau_1 = 4x, \qquad \tau_2 = 2x, \qquad \tau_3 = \frac{4x}{3},$

$$\tau_4 = 4\left(x - \frac{y}{h} \right), \quad \tau_5 = 2\left(x - \frac{y}{h} \right), \quad \tau_6 = \frac{4}{3}\left(x - \frac{y}{h} \right),$$

and H represents the Heaviside function.

The expressions for θ are:

In the horizontal strip $0 \le y \le \frac{h}{3}$

$$\theta = \left[\theta_1 (1-4x) + \theta_2 4\left(x - \frac{y}{h} \right) + \theta_7 \left(\frac{4y}{h} \right) \right] H(1-\tau_1) \qquad \left(0 \le x \le \frac{1}{3} \right),$$

$$\theta = \left(\theta_2 \left(2(1-2x) + \theta_3 \left(4x - \frac{4y}{h} - 1 \right) + \theta_6 \left(\frac{4y}{h} \right) \right) H(1-\tau_2) + \right.$$
$$\left. + \theta_2 \left(1 - \frac{4y}{h} \right) + \theta_7 \left(1 + \frac{4y}{h} - 4x \right) + \theta_6 (4x-1) \right) H(1-\tau_3) \qquad \left(\frac{1}{3} \le x \le \frac{2}{3} \right),$$

$$\theta = \theta_3 (3-4x) + 2\theta_4 \left(2x - \frac{2y}{h} - 1 \right) + \theta_6 \left(\frac{4y}{h} - 4x + 3 \right) H(1-\tau_3) +$$
$$+ \left(\theta_3 \left(1 - \frac{4y}{h} \right) + \theta_5 (4x-3) + \theta_6 \left(\frac{4y}{h} \right) \right) H(1-\tau_4) \qquad \left(\frac{2}{3} \le x \le 1 \right).$$

Along the strip $\frac{h}{3} \le y \le \frac{2h}{3}$

$$\theta=\left(\theta_7\left(2(1-2x)+\theta_6(4x-3)+\theta_8\left(\frac{4y}{h}-1\right)\right)H(1-\tau_3)+\right.$$
$$+\left(\theta_6(2\left(1-\frac{2y}{h}\right)+\theta_9\left(\frac{4y}{h}-1\right)+\theta_8\left(1+\frac{4y}{h}-4x\right)\right)H(1-\tau_4)+$$
$$+\left(\theta_6\left(4(1-x)+\theta_5\left(4x-\frac{4y}{h}-1\right)+\theta_9 2\left(\frac{4y}{h}-1\right)\right)H(1-\tau_5)\right. \qquad \left(\frac{1}{3}\le x\le\frac{2}{3}\right).$$

Along the strip $\frac{2h}{3}\le y\le 1$

$$\theta=\left(\theta_8 4(1-x)+\theta_9 4\left(x-\frac{y}{h}\right)+\theta_{10}\left(\frac{4y}{h}-3\right)\right)H(1-\tau_6) \qquad \left(\frac{2}{3}\le x\le 1\right).$$

The expressions for C are

$$C=\left(C_1(1-4x)+C_2 4\left(x-\frac{y}{h}\right)+C_7\left(\frac{4y}{h}\right)\right)H(1-\tau_1) \qquad \left(0\le x\le\frac{1}{3}\right),$$

$$C=\left(C_2\left(2(1-2x)+C_3\left(4x-\frac{4y}{h}-1\right)+C_6\left(\frac{4y}{h}\right)\right)H(1-\tau_2)+\right.$$
$$\left.+C_2\left(1-\frac{4y}{h}\right)+C_7\left(1+\frac{4y}{h}-4x\right)+C_6(4x-1)\right)H(1-\tau_3) \qquad \left(\frac{1}{3}\le x\le\frac{2}{3}\right),$$

$$C=C_3(3-4x)+2C_4\left(2x-\frac{2y}{h}-1\right)+C_6\left(\frac{4y}{h}-4x+3\right)H(1-\tau_3)+$$
$$+\left(C_3\left(1-\frac{4y}{h}\right)+C_5(4x-3)+C_6\left(\frac{4y}{h}\right)\right)H(1-\tau_4) \qquad \left(\frac{2}{3}\le x\le 1\right).$$

Along the strip $\frac{h}{3}\le y\le\frac{2h}{3}$,

$$C=\left(C_7\left(2(1-2x)+C_6(4x-3)+C_8\left(\frac{4y}{h}-1\right)\right)H(1-\tau_3)+\right.$$
$$+\left(C_6\left(2\left(1-\frac{2y}{h}\right)+C_9\left(\frac{4y}{h}-1\right)+C_8\left(1+\frac{4y}{h}-4x\right)\right)H(1-\tau_4)+\right.$$
$$+\left(C_6\left(4(1-x)+C_5\left(4x-\frac{4y}{h}-1\right)+C_9 2\left(\frac{4y}{h}-1\right)\right)H(1-\tau_5)\right. \qquad \left(\frac{1}{3}\le x\le\frac{2}{3}\right).$$

Along the strip $\frac{2c}{3}\le y\le 1$,

$$C=\left(C_8 4(1-x)+C_9 4\left(x-\frac{y}{h}\right)+C_{10}\left(\frac{4y}{h}-3\right)\right)H(1-\tau_6) \qquad \left(\frac{2}{3}\le x\le 1\right).$$

The dimensionless Nusselt numbers (Nu) and Sherwood Numbers (Sh) on the non-insulated boundary walls of the rectangular duct are calculated using the formula

$$\mathrm{Nu} = \left(\frac{\partial \theta}{\partial x}\right)_{x=1} \qquad \text{and} \qquad \mathrm{Sh} = \left(\frac{\partial C}{\partial x}\right)_{x=1}.$$

The Nusselt numbers on the side wall $x=1$ in different regions are

$$\mathrm{Nu}_1 = 2 - 4\theta_3 \qquad \left(0 \le y \le h/3\right),$$

$$\mathrm{Nu}_2 = 2 - 4\theta_5 \qquad \left(h/3 \le y \le 2h/3\right),$$

$$\mathrm{Nu}_3 = 2 - 4\theta_7 \qquad \left(2h/3 \le y \le h\right).$$

The Sherwood numbers on the side wall $x=1$ in different regions are

$$\mathrm{Sh}_1 = 2 - 4C_3 \qquad \left(0 \le y \le h/3\right),$$

$$\mathrm{Sh}_2 = 2 - 4C_5 \qquad \left(h/3 \le y \le 2h/3\right),$$

$$\mathrm{Sh}_3 = 2 - 4C_7 \qquad \left(2h/3 \le y \le h\right).$$

5. Discussion of the numerical results

We analyze the effect of radiation, dissipation and chemical reaction on the convective heat and mass transfer flow of a viscous fluid through a porous medium in a rectangular cavity. Using the Galerkin finite element analysis the governing equations are solved with linear triangular elements. The temperature, concentration, rate of heat and mass transfer are analysed for different variations of the governing parameters.

The non-dimensional temperature (θ) is shown in Figs 1-32 for different values of Ra, α, Ec, Sc, S_0, N and γ at different horizontal levels $y = \frac{h}{3}$ and $y = \frac{2h}{3}$ and vertical levels $x = \frac{1}{3}$ and $x = \frac{2}{3}$. The variation of θ with the Rayleigh number Ra is shown in Figs 1, 9, 17 and 26 at different levels. With the convention that the non-dimensional temperature is positive or negative (the actual temperature (T) is greater or lesser than T_C), it is found that the actual temperature increases with an increase in Ra at $x = \frac{1}{3}$ and $y = \frac{h}{3}$ and $y = \frac{2h}{3}$ levels. At $x = \frac{2}{3}$ level the actual temperature (T) decreases with $\mathrm{Ra} \le 2x10^2$ and increases with a higher $\mathrm{Ra} \ge 3x10^2$ (Fig.9). Figures 2, 10, 18 and 26 represent θ with the radiation parameter N_1. It is found that the higher the radiative heat flux, the larger the actual temperature and for further higher radiative heat flux, the smaller the temperature at $x = \frac{1}{3}$, $x = \frac{2}{3}$ and $y = \frac{h}{3}$ levels. At a higher horizontal level $y = \frac{2h}{3}$, the actual temperature decreases with an increase in $N_1 \le 0.03$ and increases with $N_1 \ge 0.07$ (Fig.18). Figures 3, 11, 19, and 21 represent θ with the heat source parameter α at different levels. It is found that at $x = \frac{1}{3}$, the actual temperature increases in the horizontal strip (*0*, *0.134*) and decreases in the region (*0.201*, *0.333*). At $x = \frac{2}{3}$ the actual temperature increases with an increase in $\alpha \le 4$ and for higher $\alpha \ge 6$, the actual temperature increases in the horizontal strip (*0, 0.333*) and decreases in the region (*0.391*, *0.666*). At $y = \frac{h}{3}$ level, the actual temperature decreases with α in the entire flow region. At a higher horizontal level $y = \frac{2h}{3}$ the actual temperature increases with $\alpha \le 4$ and decreases with higher $\alpha \ge 6$ (Fig.19). The effect of dissipation on θ is

shown in Figs 4, 12, 20 and 28. It is found that the actual temperature at $x=\frac{2}{3}$ and $y=\frac{2h}{3}$ increases with Ec, while at $x=\frac{1}{3}$ and $y=\frac{h}{3}$ levels the actual temperature increases with Ec ≤ *0.03* and decreases with higher Ec ≥ *0.05* (Figs 4 and 28). With respect to Sc, we find that the lesser the molecular diffusivity, the larger the actual temperature and for further lower molecular diffusivity, the smaller θ and for still lower molecular diffusivity, the larger the actual temperature at $y=\frac{h}{3}$ and $y=\frac{2h}{3}$ levels (Figs 21 and 29). At $x=\frac{1}{3}$ level, the actual temperature grows with an increase in Sc≤*0.3* and it decreases with S_0 = *1.3*, whereas at Sc = *2.01*, the actual temperature increases in the region (*0*, *0.201*), then the actual temperature decreases in the region (*0.268*. *333*) (Fig.5). From Fig.13, we notice that the actual temperature increases with lower and higher values of Sc, but at Sc =*1.3*, it decreases in the horizontal strip (*0*, *462*) and increases in the region (*0.528*, *666*). With reference to the Soret parameter S_0, we find that an increase in S_0>*0* decreases at $y=\frac{h}{3}$ and increases at $y=\frac{2h}{3}$, while with an increase $|S_0|$ (<*0*) increases at $y=\frac{h}{3}$ level and reduces at $y=\frac{2h}{3}$ level, (Figs 22 and 30). At the vertical levels $x=\frac{1}{3}$ and $x=\frac{2}{3}$ levels the actual temperature increases in the region (*0*≤*y*≤*0.201*) and it decreases in the region (*0.268*, *0.33*) with S_0>*0*, while it increases at both the levels (Figs 6 and 14). When the molecular buoyancy force dominates over the thermal buoyancy force the actual temperature increases when the buoyancy forces are in opposite directions at all horizontal and vertical levels, but for the forces acting in the same direction the actual temperature increases at $y=\frac{h}{3}$ level and decreases at $y=\frac{2h}{3}$ level. At the vertical levels: $x=\frac{1}{3}$ and $x=\frac{2}{3}$ the actual temperature reduces in the horizontal strip (*0*, *0.134*) and increases in the strip (*0.201*, *0.333*) (Figs 7 and 15). The variation of θ with the chemical reaction parameter γ is shown in Figs 8, 16, 24, and 32. At $y=\frac{h}{3}$ and $x=\frac{1}{3}$ the actual temperatures decrease in the case of a chemical reaction. At $y=\frac{2h}{3}$ and $x=\frac{2}{3}$ the actual temperature decreases with γ≤*0.5* and increases with γ≥*2.0*, while at $y=\frac{2h}{3}$, it reduces with |γ| ≤ *0.5*, grows with |γ| ≥ *2* and at $x=\frac{2}{3}$, it reduces with |γ|≤*0.5* and reduces with |γ|≥*2* at $x=\frac{1}{3}$, an increase in γ ≤ *0.5*, enhances the actual temperature in the horizontal strip (*0*, *0.201*) and reduces it in the region (*0.268*, *0.333*). At $y=\frac{h}{3}$ level, an increase in γ≤*0.5*, enhances the actual temperature in the region (*0.333*, *0.663*) and reduces in the region (*0.729*, *1*) and for higher γ≥*2*, a reversed effect is noticed in the behavior of the actual temperature (Fig.32).

The non-dimensional concentration (*C*) is shown in Figs 33-64 for different parametric values at different horizontal and vertical levels. Figures 33, 41, 49 and 58 represent the concentration (*C*) with the Rayleigh number Ra. The concentration enhances at $x=\frac{1}{3}$ level and depreciates at $y=\frac{2h}{3}$ level. At $y=\frac{h}{3}$ level it reduces with Ra≤$2x10^2$ and enhances with higher Ra≥$3x10^2$. At $x=\frac{2}{3}$ with an increase in Ra≤$2x10^2$

the concentration (C) decreases in the region (*0*, *0.264*) and grows in the region (*0.33≤y≤ 0.666*) while for higher Ra≥*3x10*^{2}, the concentration increases in the region (*0*, *0.264*) and decreases in the region (*0.33*, *0.666*) (Fig.41). The effect of radiation on C is shown in Figs 34, 42, 50 and 58. At $y=\frac{h}{3}$ and $x=\frac{2}{3}$ levels the actual concentration increases with an increase in the radiation parameter N_1 (Figs 42 and 58). At $y=\frac{2h}{3}$ level, it decreases with $N_1\leq 0.03$ and grows with $N_1\geq 0.05$ (Fig.50). At $x=\frac{1}{3}$ level the concentration increases with $N_1\leq 0.03$ and for higher $N_1\geq 0.05$, it decreases in the horizontal strip (*0*, *0.201*) and grows in the strip (*0.268*, *0.333*) (Fig.34). With respect to the heat source parameter α we find that the actual concentration grows with an increase in α≤*4* and reduces with higher α≥*6* at $y=\frac{h}{3}$ and $y=\frac{2h}{3}$ levels. At $x=\frac{1}{3}$ level the concentration grows with α≤*4* and for α≥*6*, it reduces in the horizontal strip (*0*, *0.268*) except in a narrow region adjacent to *y =0.333* (Fig.35). At $x=\frac{2}{3}$ level, the concentration increases in the horizontal region (*0*, *0.264*) and reduces in the region (*0.33*, *0.666*) for α≤*4* and reduces in the entire flow region for α≥*6* (Fig.43). The effect of dissipation on C is shown in Figs 36, 44, 52 and 60. It is found that at horizontal levels $y=\frac{h}{3}$ and $y=\frac{2h}{3}$ and vertical level $x=\frac{1}{3}$, the actual concentration decreases with Ec≤*0.03* and grows with higher Ec≥*0.05* (Figs 36, 52 and 60). At $x=\frac{2}{3}$ level the actual concentration grows with Ec≤*0.03* except in the region (*0.396*, *0.462*) and for higher Ec≥*0.05*, the concentration grows in the region (*0*, *0.396*) and reduces in the region (*0.462*, *0.666*) (Fig.44). The effect of the Schmidt number Sc on C is shown in Figs 37, 45, 53, 61. The lesser molecular diffusivity, the larger is the actual concentration at $y=\frac{2h}{3}$ level. At $y=\frac{h}{3}$ level, the actual concentration grows with Sc≤*1.3* and decreases with Sc≥*2.01* (Fig.61). At $x=\frac{1}{3}$ level the actual concentration decreases with Sc = *0.6* and grows with Sc at *y = 0* and in the remaining region it grows at Sc = *0.6*, then decreases with Sc = *2.01* (Fig.37). At $x=\frac{2}{3}$ level, for lower (Sc=*0.6*) and higher values of Sc =*2.01* the actual concentration decreases in the region (*0*, *0.333*) and grows in the region (*0.396*, *0.666*), while at Sc =*1.3*, it depreciates in the strip (*0.396*, *0.666*) (Fig.45). With respect to the Soret parameter S_0, we find that the actual concentration grows with $|S_0|$ at all horizontal levels and vertical level at $x=\frac{1}{3}$ (Figs 38, 54, 62). At the vertical level $x=\frac{2}{3}$, the concentration grows in the region (*0*, *0.333*) and depreciates in the region (*0.462*, *0.666*) (Fig.46). When the molecular buoyancy force dominates over the thermal buoyancy force, the actual concentration at $x=\frac{1}{3}$, $y=\frac{h}{3}$ and $y=\frac{2h}{3}$ levels decreases irrespective of the directions of the buoyancy forces (Figs 39, 55 and 63). At $x=\frac{2}{3}$ level the actual concentration reduces in the horizontal strip (*0.462*, *0.666*) with an increase in *N>0* and depreciates with |*N*| (*<0*) (Fig.47). The variation of C with the chemical reaction parameter γ is shown in Figs 40, 48, 56 and 64. It is found that the actual concentration decreases at $x=\frac{1}{3}$, $x=\frac{2}{3}$ and $y=\frac{h}{3}$ levels and grows at $y=\frac{2h}{3}$ in the case of a chemical reaction. In the

case of no chemical reaction the actual concentration grows at $y=\frac{h}{3}$ level and decreases at $y=\frac{2h}{3}$ level with $\gamma \le 0.5$, but a reversed effect is noticed at $\gamma = 2$ (Figs 56 and 64). At the vertical level $x=\frac{2}{3}$, the actual concentration grows in the strip (*0*, *0.264*) and reduces in the strip (*0.33*, *0.666*) for $\gamma \le 0.5$ and for higher $\gamma \ge 2$, we notice depreciation in the entire flow region ($0 \le y \le 0.666$) (Fig.48).

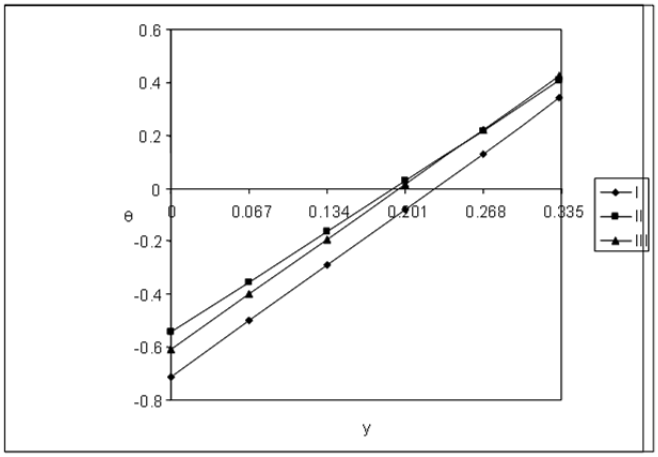

Fig.1. Variation of θ with Ra at $x=\frac{1}{3}$ level

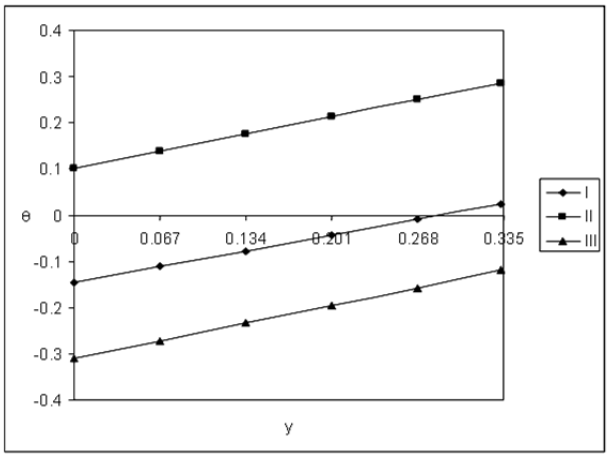

Fig.2. Variation of θ with Ra at $x=\frac{1}{3}$ level

	I	II	III
Ra	10^2	2×10^2	3×10^2

	I	II	III
Rad	*0.01*	*0.03*	*0.07*

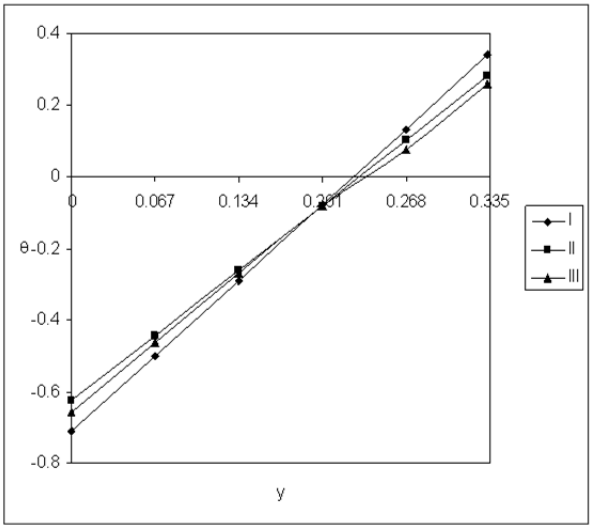

Fig.3. Variation of θ with α at $x=\frac{1}{3}$ level

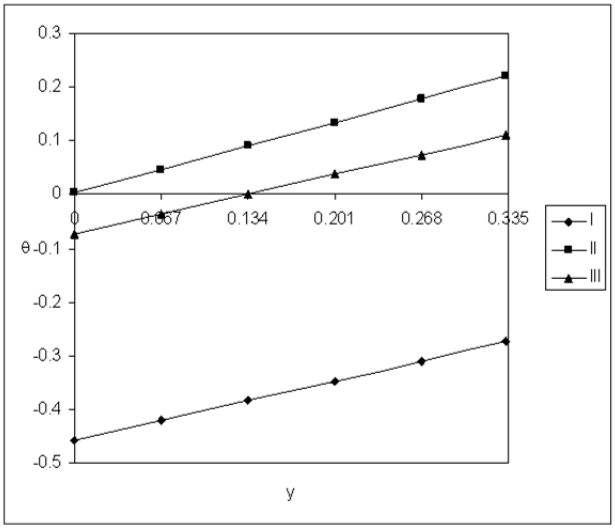

Fig.4. Variation of θ with Ec at $x=\frac{1}{3}$ level

	I	II	III
α	*2*	*4*	*6*

	I	II	III
Ec	*0.001*	*0.003*	*0.005*

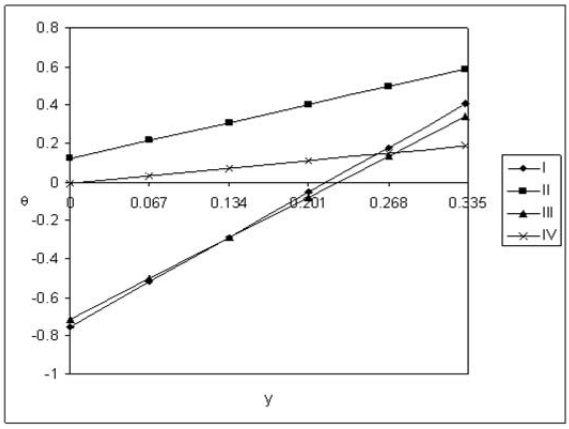

Fig.5. Variation of θ with Sc at $x = \frac{1}{3}$ level

	I	II	III	IV
Sc	*0.24*	*0.6*	*1.3*	*2.01*

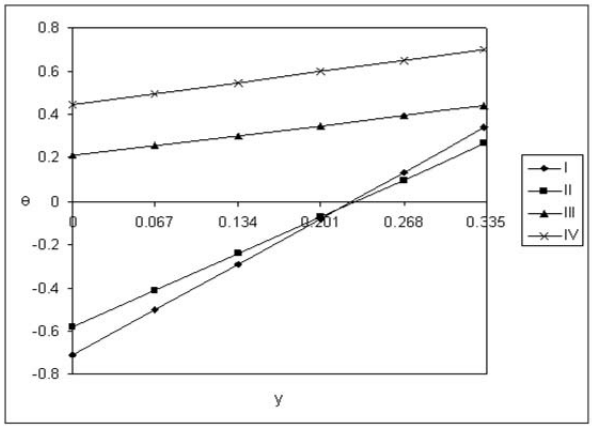

Fig.6. Variation of θ with S_0 at $x = \frac{1}{3}$ level

	I	II	III	IV
S_0	*0.5*	*1*	*–0.5*	*–1*

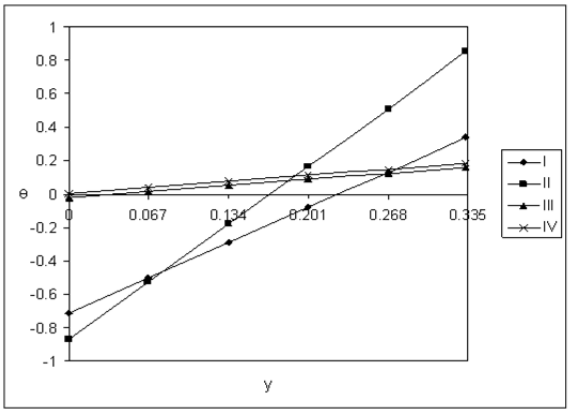

Fig.7. Variation of θ with N at $x = \frac{1}{3}$ level

	I	II	III	IV
N	*1*	*2*	*–0.5*	*–0.8*

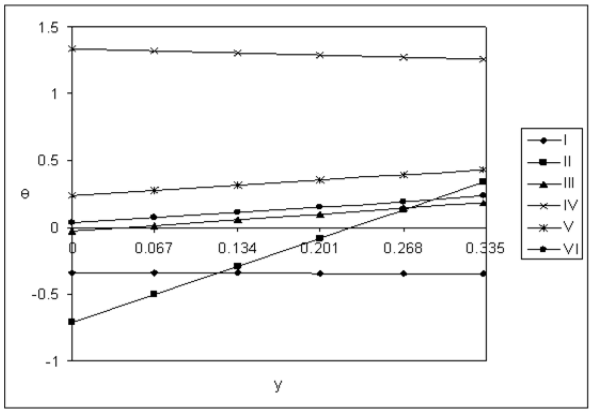

Fig.8. Variation of θ with γ at $x = \frac{1}{3}$ level

	I	II	III	IV	V	VI
γ	*0.2*	*0.5*	*2*	*–0.2*	*–0.5*	*–2*

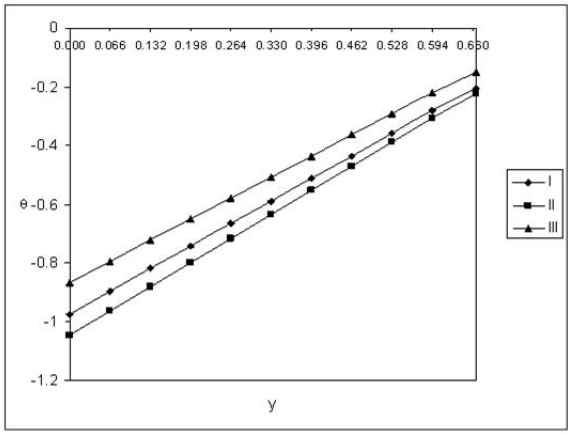

Fig.9. Variation of θ with Ra at $x = \frac{2}{3}$ level

	I	II	III
Ra	10^2	2×10^2	3×10^2

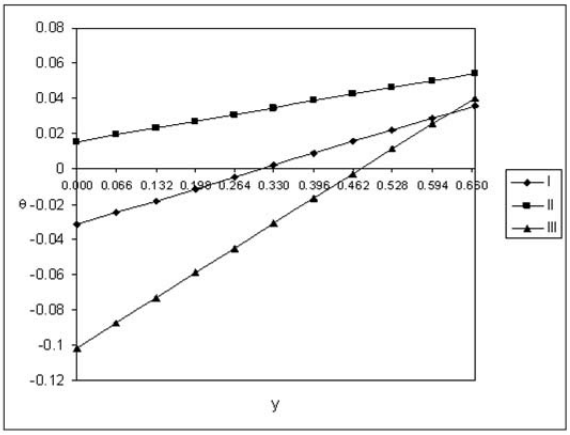

Fig.10. Variation of θ with Ra at $x = \frac{2}{3}$ level

	I	II	III
Rad	*0.01*	*0.03*	*0.07*

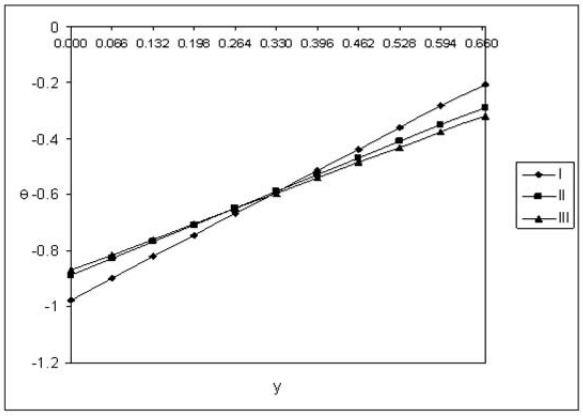

Fig.11. Variation of θ with α at $x=\frac{2}{3}$ level

	I	II	III
α	*2*	*4*	*6*

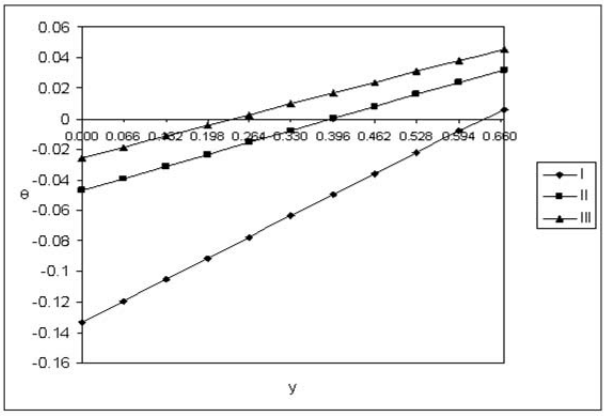

Fig.12. Variation of θ with Ec at $x=\frac{2}{3}$ level

	I	II	III
Ec	*0.001*	*0.003*	*0.005*

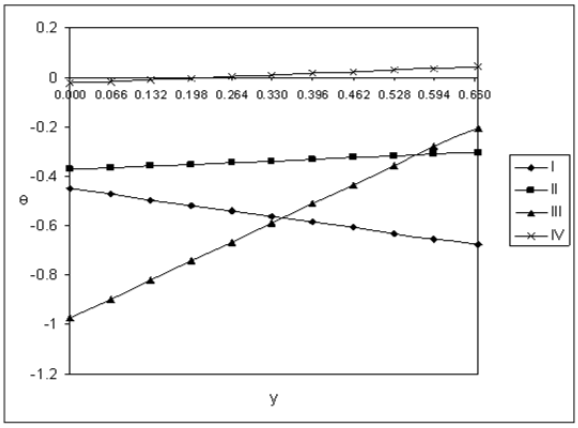

Fig.13. Variation of θ with Sc at $x=\frac{2}{3}$ level

	I	II	III	IV
Sc	*0.24*	*0.6*	*1.3*	*2.01*

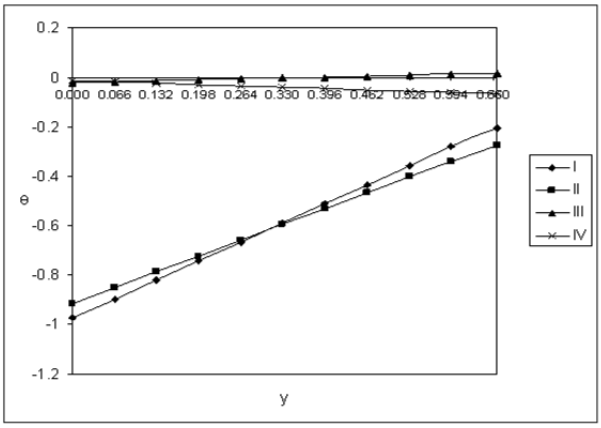

Fig.14. Variation of θ with S_0 at $x=\frac{2}{3}$ level

	I	II	III	IV
S_0	*0.5*	*1*	*−0.5*	*−1*

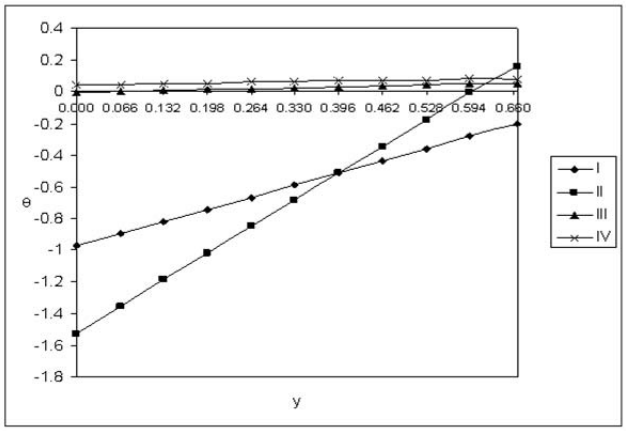

Fig.15. Variation of θ with *N* at $x=\frac{2}{3}$ level

	I	II	III	IV
N	*1*	*2*	*−0.5*	*−0.8*

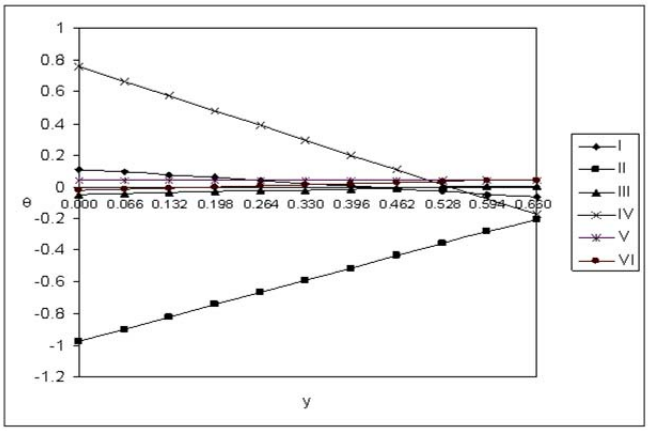

Fig.16. Variation of θ with γ at $x=\frac{2}{3}$ level

	I	II	III	IV	V	VI
γ	*0.2*	*0.5*	*2*	*−0.2*	*−0.5*	*−2*

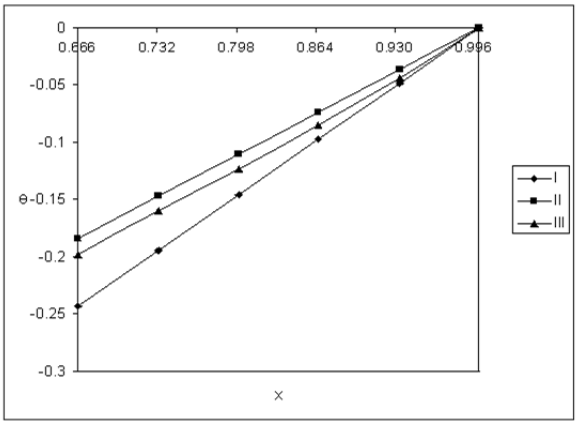

Fig.17. Variation of θ with Ra at $y=\frac{2h}{3}$ level

	I	II	III
Ra	10^2	2×10^2	3×10^2

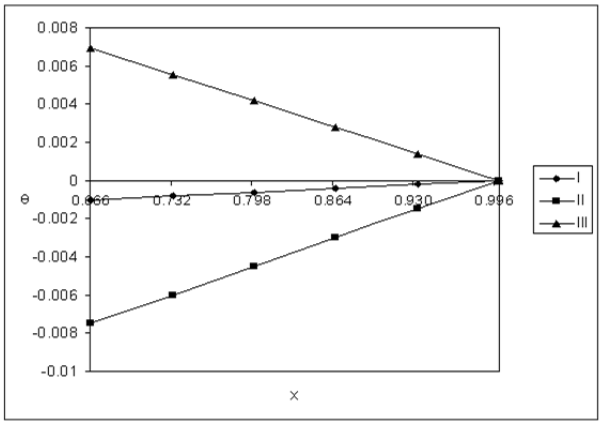

Fig.18. Variation of θ with Ra at $y=\frac{2h}{3}$ level

	I	II	III
Rad	*0.01*	*0.03*	*0.07*

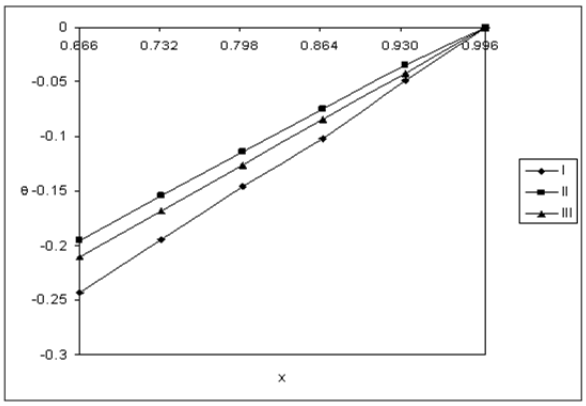

Fig.19. Variation of θ with α at $y=\frac{2h}{3}$ level

	I	II	III
α	*2*	*4*	*6*

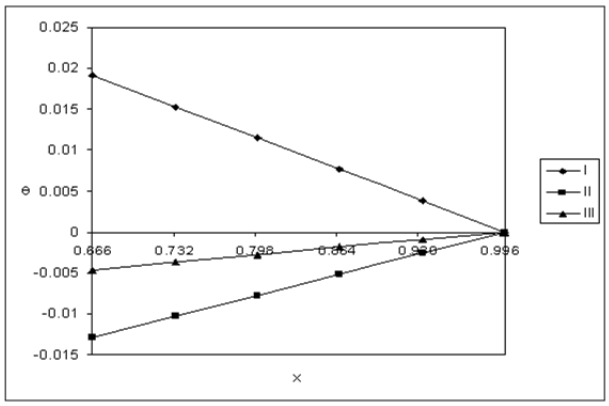

Fig.20. Variation of θ with Ec at $y=\frac{2h}{3}$ level

	I	II	III
Ec	*0.001*	*0.003*	*0.005*

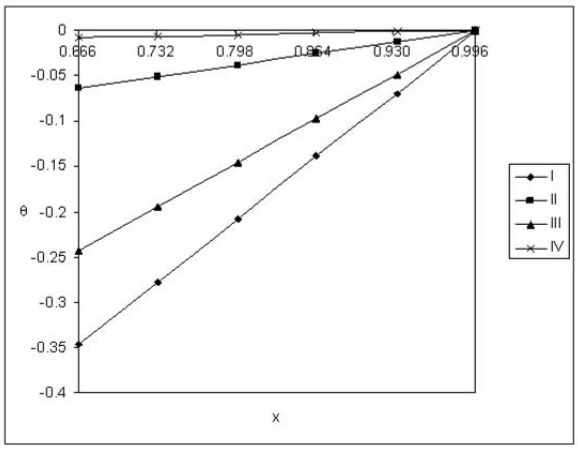

Fig.21. Variation of θ with Sc at $y=\frac{2h}{3}$ level

	I	II	III	IV
Sc	*0.24*	*0.6*	*1.3*	*2.01*

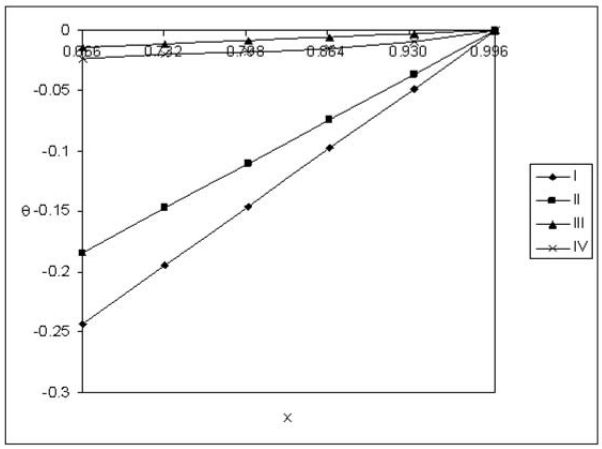

Fig.22. Variation of θ with S_0 at $y=\frac{2h}{3}$ level

	I	II	III	IV
S_0	*0.5*	*1*	*–0.5*	*–1*

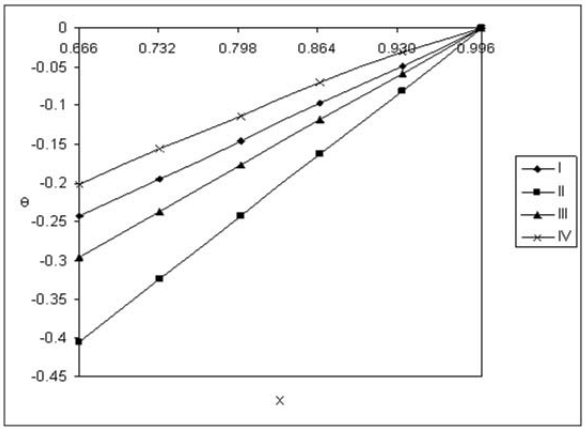

Fig.23. Variation of θ with N at $y=\frac{2h}{3}$ level

	I	II	III	IV
N	*1*	*2*	*–0.5*	*–0.8*

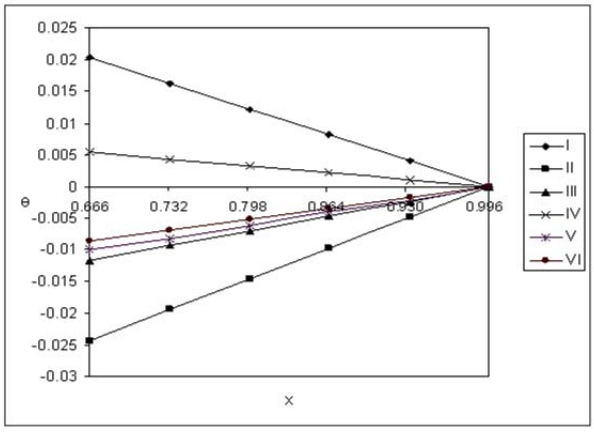

Fig.24. Variation of θ with γ at $y=\frac{2h}{3}$ level

	I	II	III	IV	V	VI
γ	*0.2*	*0.5*	*2*	*–0.2*	*–0.5*	*–2*

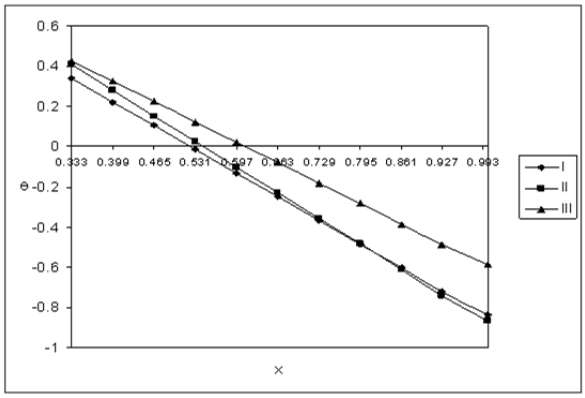

Fig.25. Variation of θ with Ra at $y=\frac{h}{3}$ level

	I	II	III
Ra	10^2	2×10^2	3×10^2

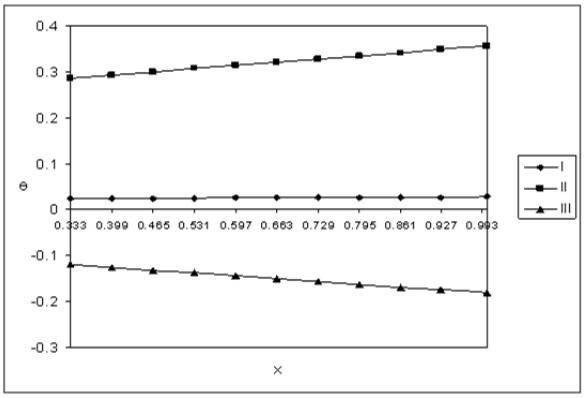

Fig.26. Variation of θ with Ra at $y=\frac{h}{3}$ level

	I	II	III
Rad	*0.01*	*0.03*	*0.07*

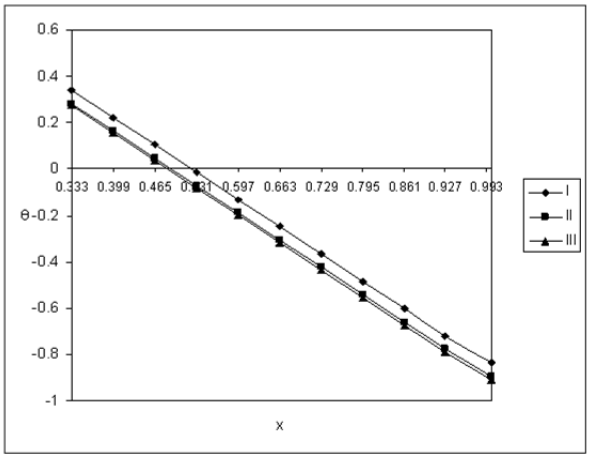

Fig.27. Variation of θ with α at $y=\frac{h}{3}$ level

	I	II	III
α	*2*	*4*	*6*

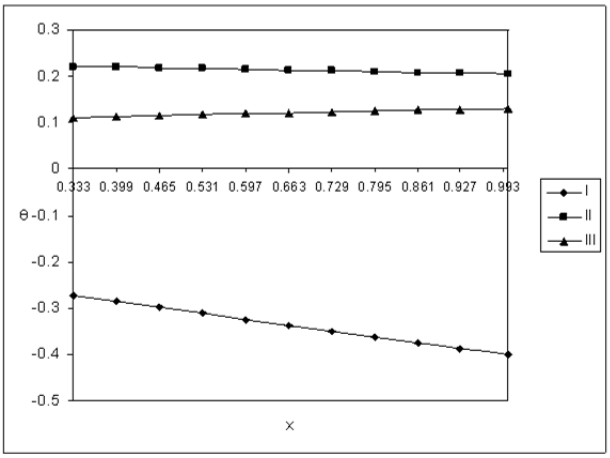

Fig.28. Variation of θ with Ec at $y=\frac{h}{3}$ level

	I	II	III
Ec	*0.001*	*0.003*	*0.005*

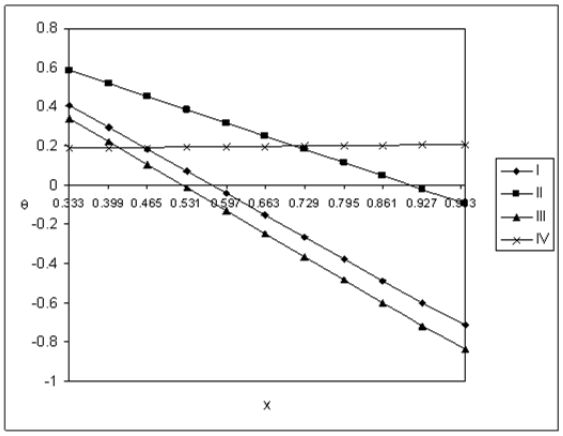

Fig.29. Variation of θ with Sc at $y = \frac{h}{3}$ level

	I	II	III	IV
Sc	*0.24*	*0.6*	*1.3*	*2.01*

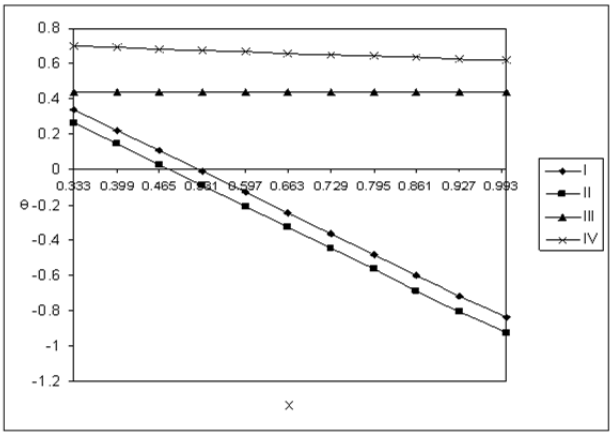

Fig.30. Variation of θ with S_0 at $y = \frac{h}{3}$ level

	I	II	III	IV
S_0	*0.5*	*1*	*–0.5*	*–1*

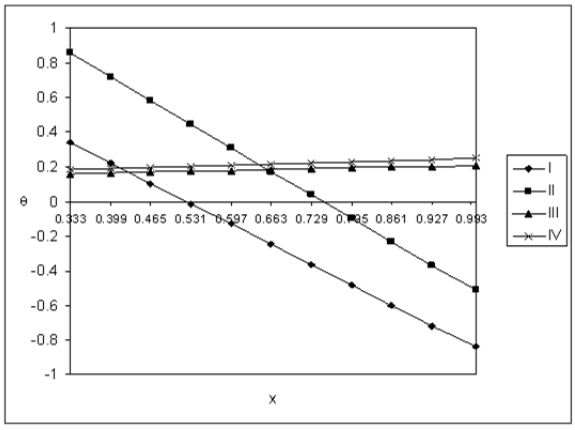

Fig.31. Variation of θ with *N* at $y = \frac{h}{3}$ level

	I	II	III	IV
N	*1*	*2*	*–0.5*	*–0.8*

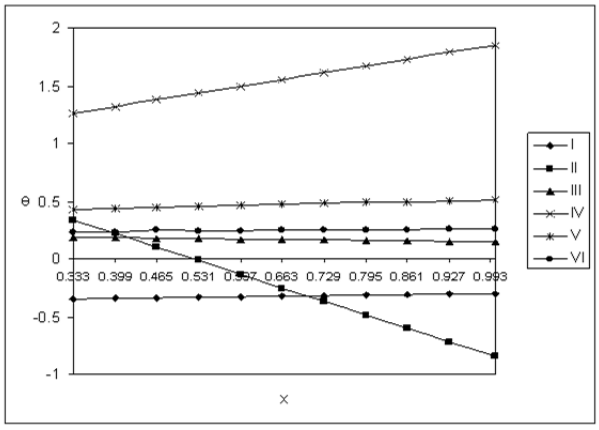

Fig.32. Variation of θ with γ at $y = \frac{h}{3}$ level

	I	II	III	IV	V	VI
γ	*0.2*	*0.5*	*2*	*–0.2*	*–0.5*	*–2*

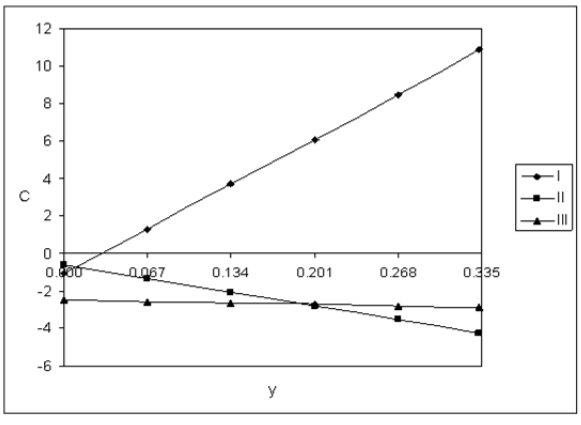

Fig.33. Variation of C with Ra at $x = \frac{1}{3}$ level

	I	II	III
Ra	10^2	2×10^2	3×10^2

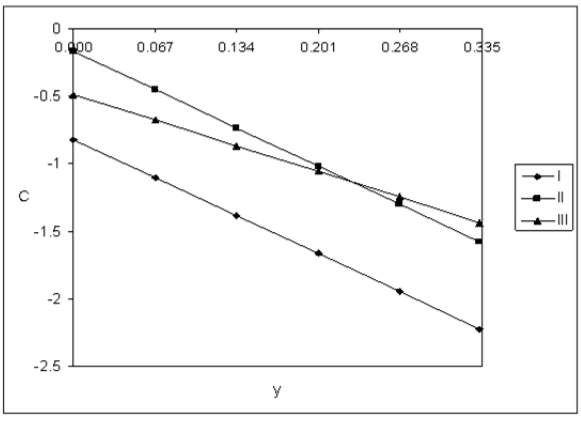

Fig.34. Variation of C with Ra at $x = \frac{1}{3}$ level

	I	II	III
Rad	*0.01*	*0.03*	*0.07*

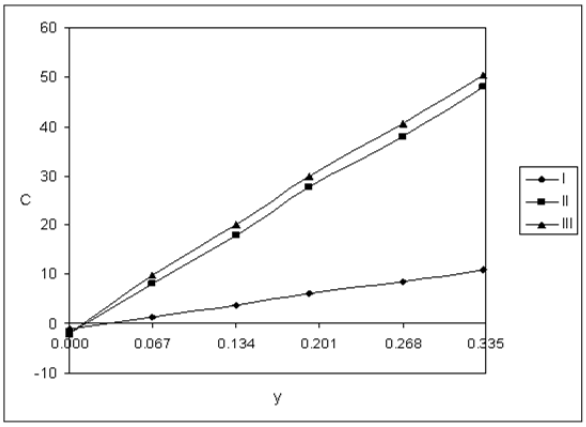

Fig.35. Variation of C with α at $x=\frac{1}{3}$ level

I II III
α *2 4 6*

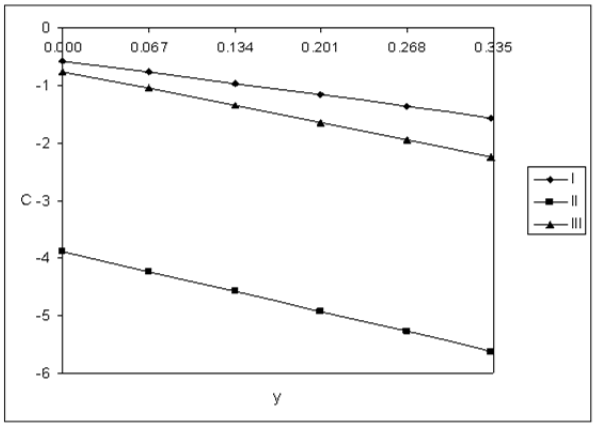

Fig.36. Variation of C with Ec at $x=\frac{1}{3}$ level

I II III
Ec *0.001 0.003 0.005*

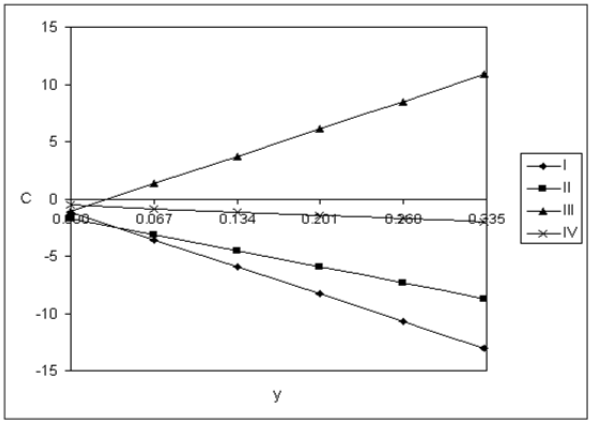

Fig.37. Variation of C with Sc at $x=\frac{1}{3}$ level

I II III IV
Sc *0.24 0.6 1.3 2.01*

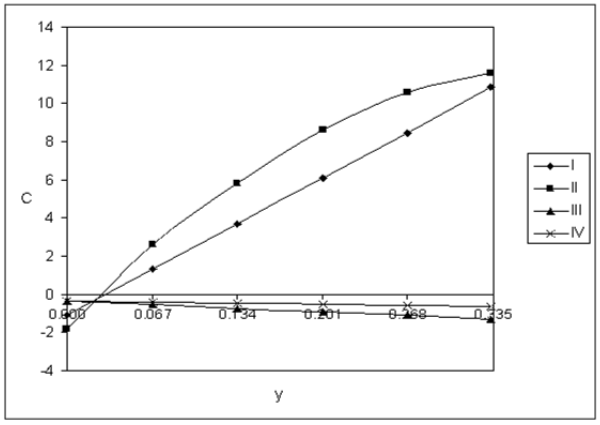

Fig.38. Variation of C with S_0 at $x=\frac{1}{3}$ level

I II III IV
S_0 *0.5 1 –0.5 –1*

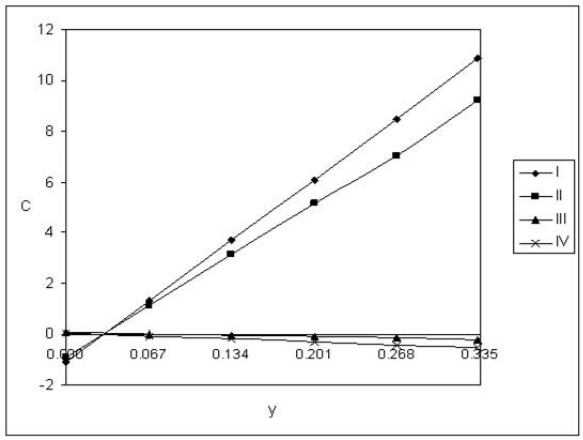

Fig.39. Variation of C with N at $x=\frac{1}{3}$ level

I II III IV
N *1 2 –0.5 –0.8*

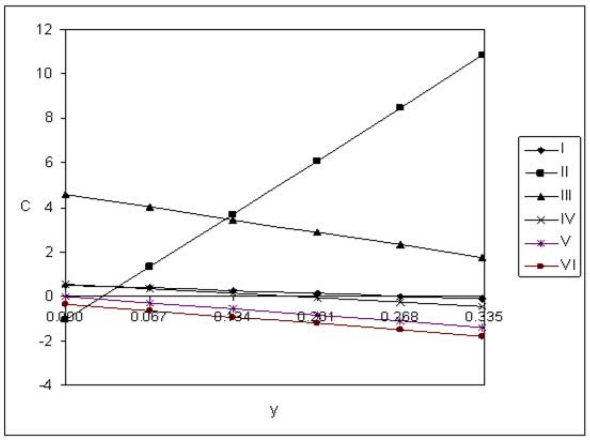

Fig.40. Variation of C with γ at $x=\frac{1}{3}$ level

I II III IV V VI
γ *0.2 0.5 2 –0.2 –0.5 –2*

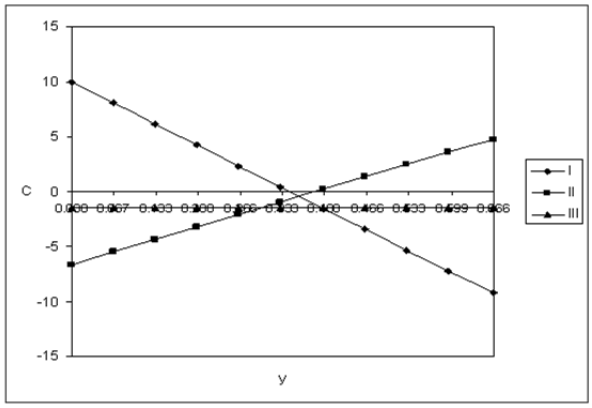

Fig.41. Variation of C with Ra at $x=\frac{2}{3}$ level

I II III

Ra 10^2 2×10^2 3×10^2

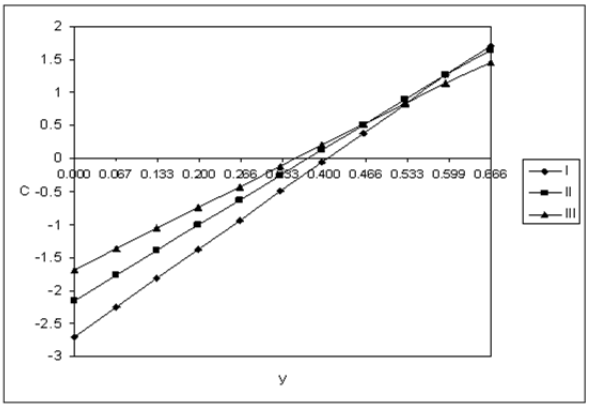

Fig.42. Variation of C with Ra at $x=\frac{2}{3}$ level

I II III

Rad *0.01* *0.03* *0.07*

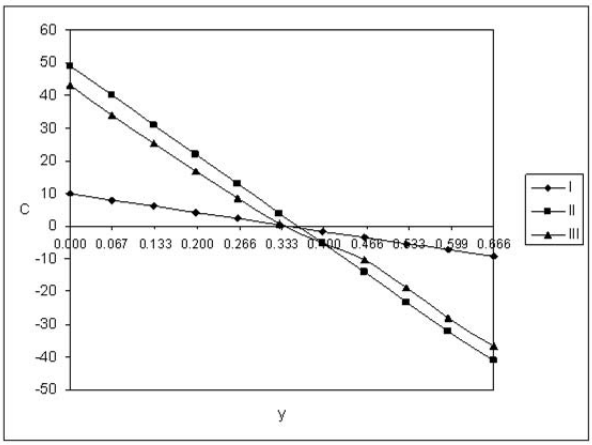

Fig.43. Variation of C with α at $x=\frac{2}{3}$ level

I II III

α *2* *4* *6*

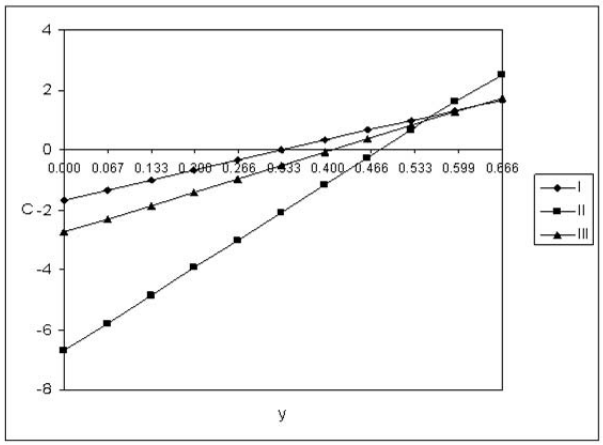

Fig.44. Variation of C with Ec at $x=\frac{2}{3}$ level

I II III

Ec *0.001* *0.003* *0.005*

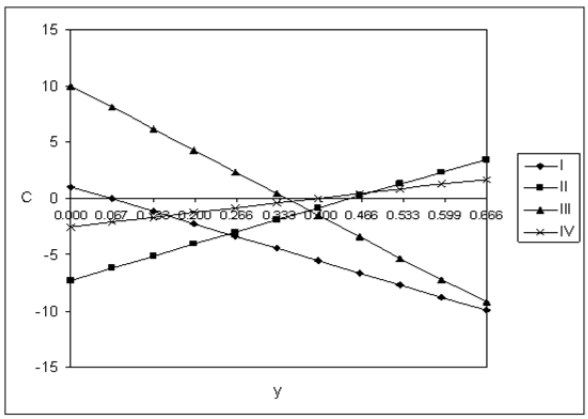

Fig.45. Variation of C with Sc at $x=\frac{2}{3}$ level

I II III IV

Sc *0.24* *0.6* *1.3* *2.01*

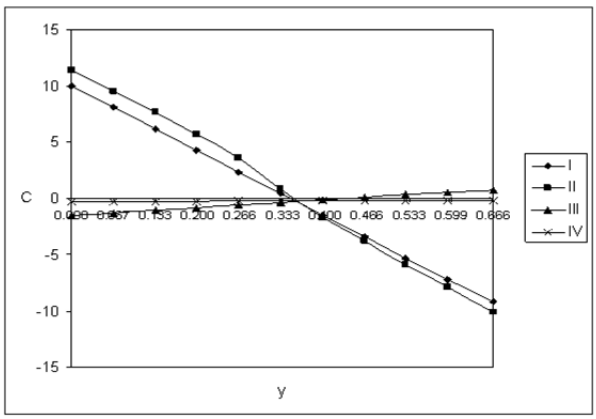

Fig.46. Variation of C with S_0 at $x=\frac{2}{3}$ level

I II III IV

S_0 *0.5* *1* *–0.5* *–1*

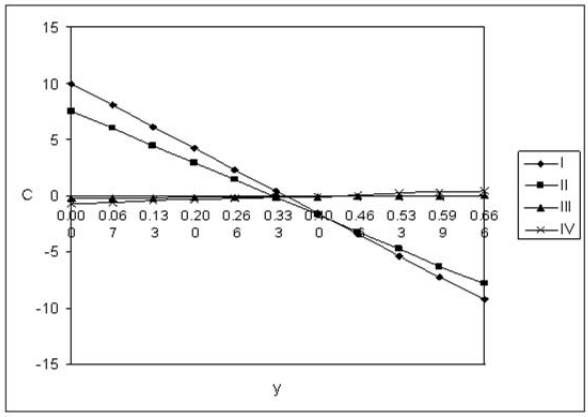

Fig.47. Variation of C with N at $x=\frac{2}{3}$ level

	I	II	III	IV
N	1	2	−0.5	−0.8

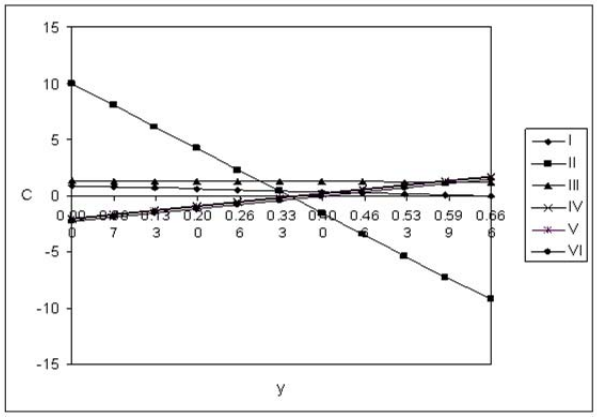

Fig.48. Variation of C with γ at $x=\frac{2}{3}$ level

	I	II	III	IV	V	VI
γ	0.2	0.5	2	−0.2	−0.5	−2

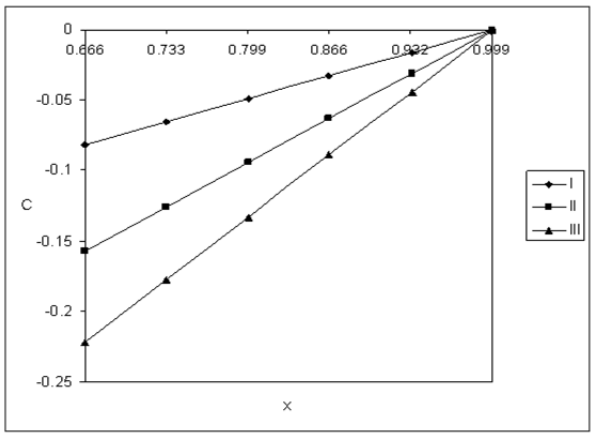

Fig.49. Variation of C with Ra at $y=\frac{2h}{3}$ level

	I	II	III
Ra	10^2	2×10^2	3×10^2

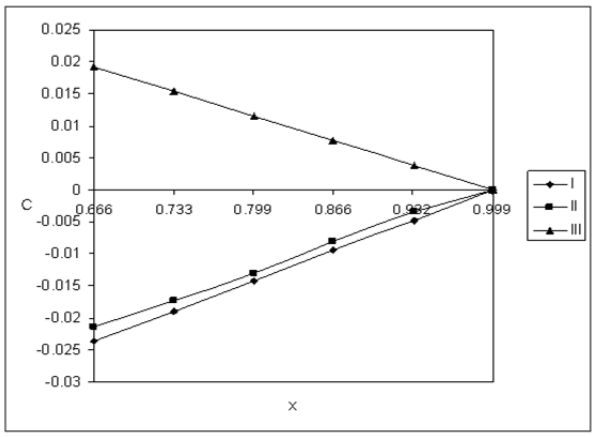

Fig.50. Variation of C with Ra at $y=\frac{2h}{3}$ level

	I	II	III
Rad	0.01	0.03	0.07

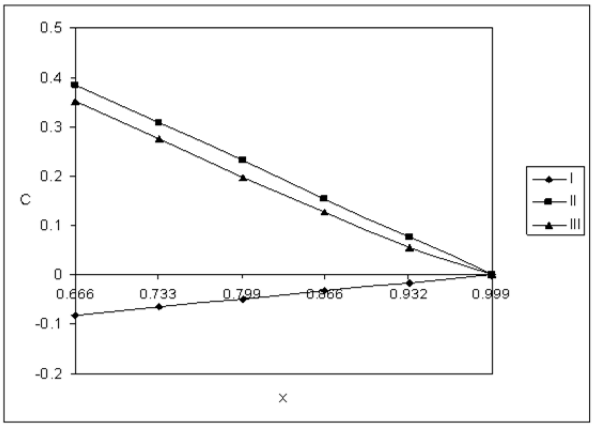

Fig.51. Variation of C with α at $y=\frac{2h}{3}$ level

	I	II	III
α	2	4	6

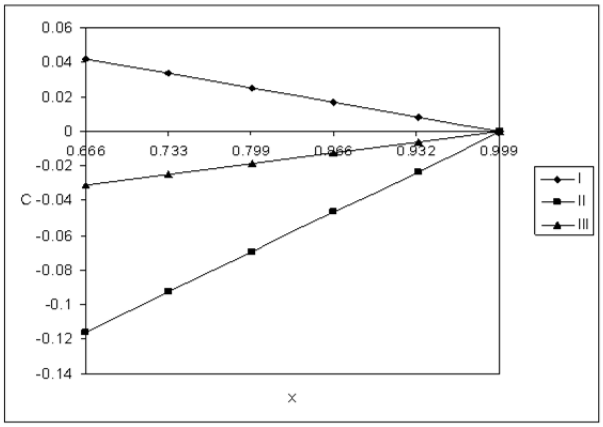

Fig.52. Variation of C with Ec at $y=\frac{2h}{3}$ level

	I	II	III
Ec	0.001	0.003	0.005

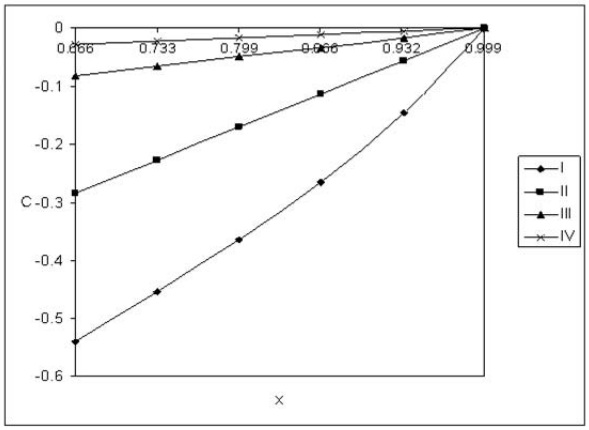

Fig.53. Variation of C with Sc at $y=\frac{2h}{3}$ level

	I	II	III	IV
Sc	*0.24*	*0.6*	*1.3*	*2.01*

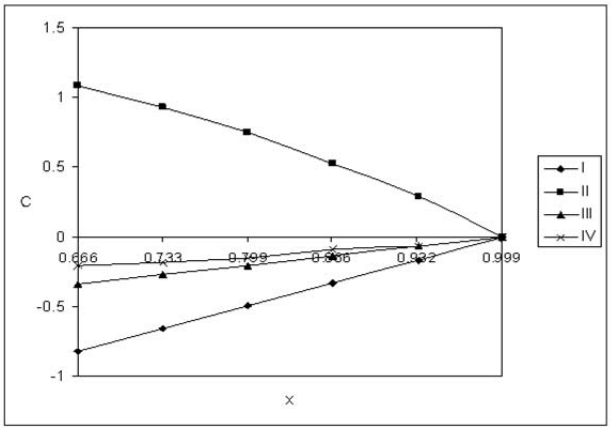

Fig.54. Variation of C with S_0 at $y=\frac{2h}{3}$ level

	I	II	III	IV
S_0	*0.5*	*1*	*–0.5*	*–1*

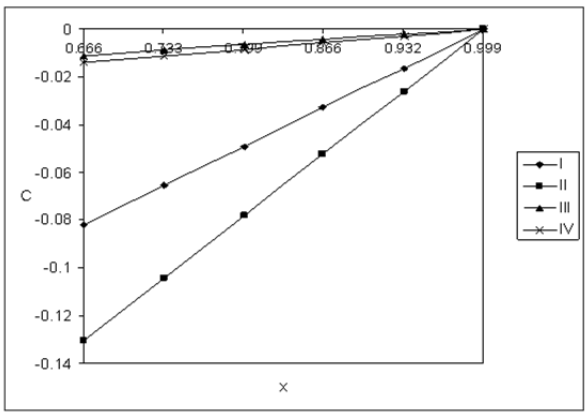

Fig.55. Variation of C with N at $y=\frac{2h}{3}$ level

	I	II	III	IV
N	*1*	*2*	*–0.5*	*–0.8*

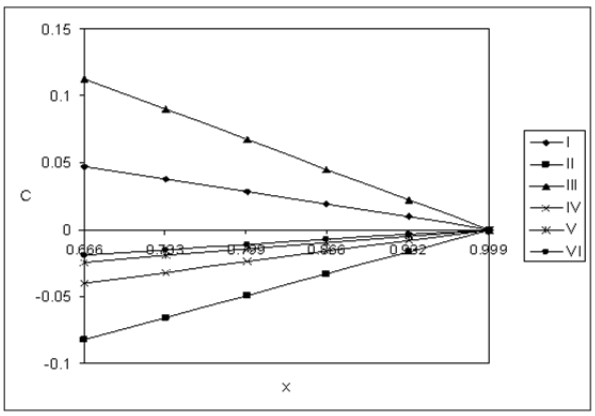

Fig.56. Variation of C with γ at $y=\frac{2h}{3}$ level

	I	II	III	IV	V	VI
γ	*0.2*	*0.5*	*2*	*–0.2*	*–0.5*	*–2*

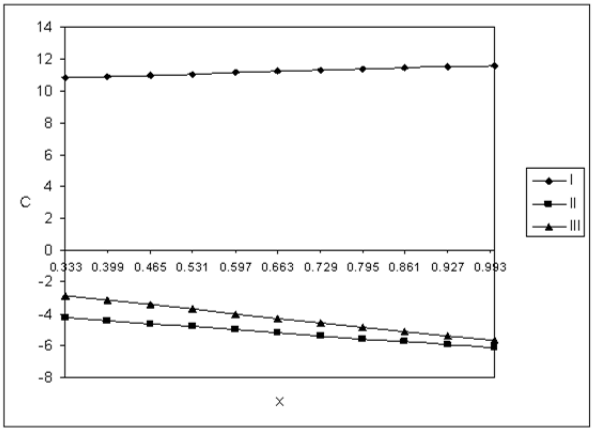

Fig.57. Variation of C with Ra at $y=\frac{h}{3}$ level

	I	II	III
Ra	10^2	2×10^2	3×10^2

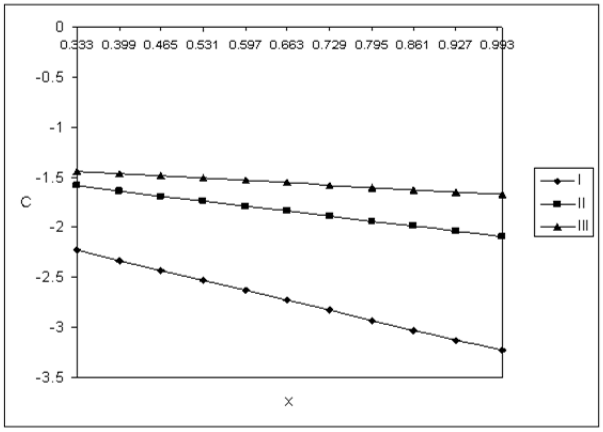

Fig.58. Variation of C with Ra at $y=\frac{h}{3}$ level

	I	II	III
Rad	*0.01*	*0.03*	*0.07*

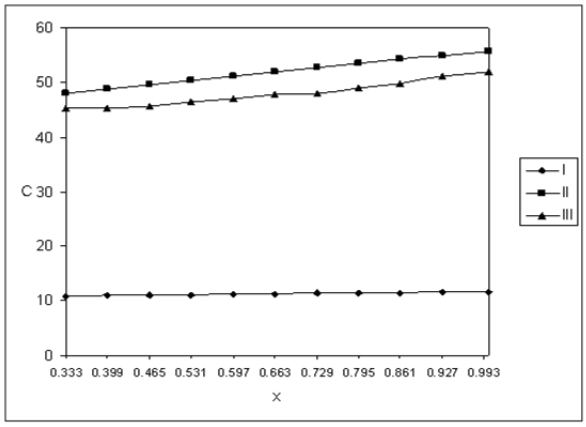

Fig.59. Variation of C with α at $y = \frac{h}{3}$ level

	I	II	III
α	*2*	*4*	*6*

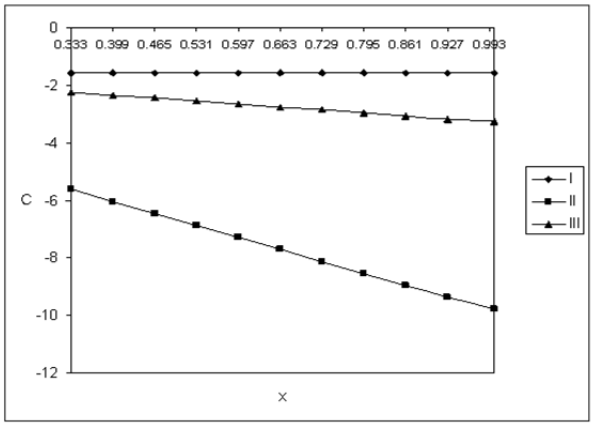

Fig.60. Variation of C with Ec at $y = \frac{h}{3}$ level

	I	II	III
Ec	*0.001*	*0.003*	*0.005*

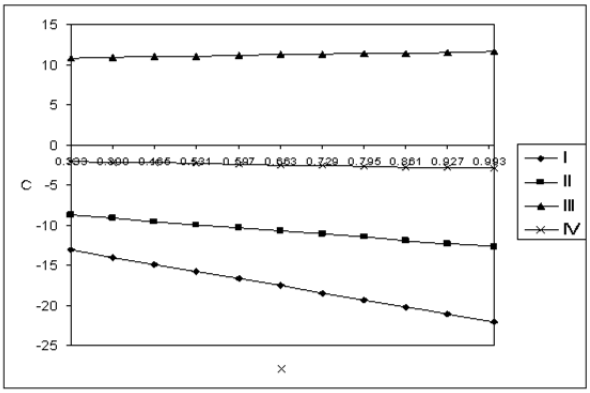

Fig.61. Variation of C with Sc at $y = \frac{h}{3}$ level

	I	II	III	IV
Sc	*0.24*	*0.6*	*1.3*	*2.01*

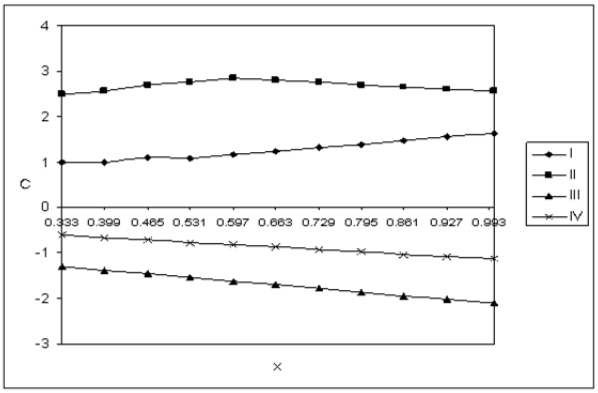

Fig.62. Variation of C with S_0 at $y = \frac{h}{3}$ level

	I	II	III	IV
S_0	*0.5*	*1*	*–0.5*	*–1*

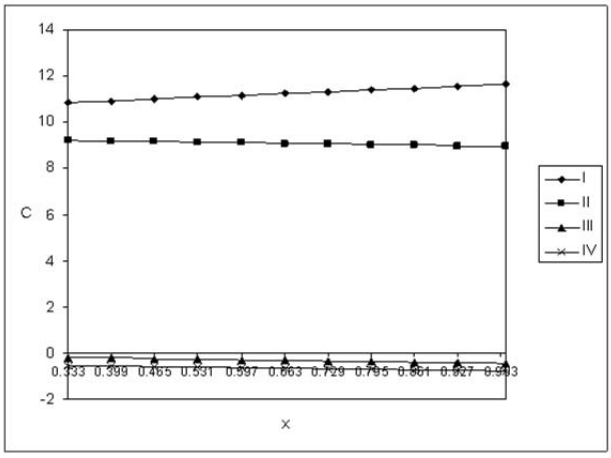

Fig.63. Variation of C with N at $y = \frac{h}{3}$ level

	I	II	III	IV
N	*1*	*2*	*–0.5*	*–0.8*

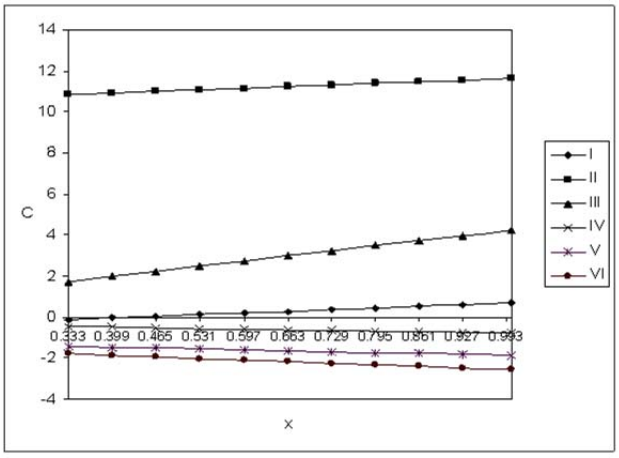

Fig.64. Variation of C with γ at $y = \frac{h}{3}$ level

	I	II	III	IV	V	VI
γ	*0.2*	*0.5*	*2*	*–0.2*	*–0.5*	*–2*

The rate of heat transfer (Nu) at $x = 1$ is shown in Tabs 1-3 for different levels. Table 1 shows the variation of Nu with the Rayleigh number Ra and heat source parameter α. It is found that the rate of heat transfer increases with an increase in $Ra \leq 2x10^2$ and depreciates with higher $Ra \geq 3x10^2$ in all the three quadrants. With respect to α, we find that the Nusselt number decreases in the lower and middle quadrants and increases in the upper quadrant with an increase in α. When the molecular buoyancy force dominates over the thermal buoyancy force the Nusselt number grows in the lower and middle quadrants and depreciates in the upper quadrant when the buoyancy forces act in the same directions and for the forces acting in opposite directions, |Nu| decreases at all the three quadrants with respect to the Schmidt number Sc. We find that the lesser the molecular diffusivity, the larger |Nu| and for still lower molecular diffusivity, the larger |Nu| at all the quadrants. The variation of Nu with the Soret parameter S_0 shows that the rate of heat transfer decreases with $|S_0|$ in the first quadrant and increases with $|S_0|$ in the middle and upper quadrants (Tab.2). With respect to the radiation parameter N_1 we find that the Nusselt number decreases with $N_1 \leq 0.03$ and increases with higher $N_1 \geq 0.07$ in all the quadrants. The higher the dissipative heat, the smaller |Nu| and for further higher dissipative heat ($Ec \geq 0.005$), the larger |Nu| in all the three quadrants. The variation of Nu with the chemical reaction parameter γ shows that the Nusselt number in all the three quadrants increases with $\gamma \leq 1.5$ and decreases with higher $\gamma \geq 2.5$. In the generating chemical reaction case the Nusselt number in the lower and middle quadrants grows with $|\gamma|$ while in the upper quadrant, it depreciates with $|\gamma| \leq 1.5$ and grows with $|\gamma| \geq 2.5$ (Tab.3).

Table 1. Nusselt number (Nu) at different levels.

	I	II	III	IV	V
Nu1	*5.89625*	*6.19412*	*5.46543*	*5.54957*	*5.4746*
Nu2	*4.35776*	*4.54913*	*4.03072*	*4.23018*	*4.374*
Nu3	*2.81926*	*2.88152*	*2.596*	*3.15086*	*3.2734*
Ra	10^2	2×10^2	3×10^2	10^2	10^2
α	*2*	*2*	*2*	*4*	*6*

Table 2. Nusselt number (Nu) at different levels.

	I	II	III	IV	V	VI	VII	VIII	IX	X
Nu1	*5.89625*	*8.09168*	*2.01284*	*1.969*	*3.8048*	*3.48837*	*2.09389*	*5.6592*	*2.08116*	*2.0535*
Nu2	*4.35776*	*4.72671*	*1.89901*	*1.86854*	*4.254*	*3.35474*	*1.96231*	*4.3808*	*2.00948*	*2.124146*
Nu3	*2.81926*	*1.35575*	*1.78519*	*1.76807*	*4.7032*	*3.22112*	*1.83072*	*3.1024*	*1.95224*	*2.2684*
N	*1*	*2*	*-0.5*	*-0.8*	*1*	*1*	*1*	*1*	*1*	*1*
Sc	*1.3*	*1.3*	*1.3*	*1.3*	*0.24*	*0.6*	*2.01*	*1.3*	*1.3*	*1.3*
S0	*0.5*	*0.5*	*0.5*	*0.5*	*0.5*	*0.5*	*0.5*	*1*	*-0.5*	*-1*

Table 3. Nusselt number (Nu) at different levels.

	I	II	III	IV	V	VI	VII	VIII	IX	X	XI
Nu1	*2.12654*	*1.93846*	*2.40676*	*2.18783*	*2.103*	*1.55902*	*5.89625*	*2.18555*	*-1.0392*	*1.83438*	*2.075676*
Nu2	*1.99172*	*1.86078*	*2.12364*	*2.0305*	*1.9609*	*1.90722*	*4.35776*	*2.07458*	*0.82518*	*1.829688*	*1.951196*
Nu3	*1.85689*	*1.78312*	*1.8405*	*1.87318*	*1.8187*	*2.25541*	*2.81926*	*1.96362*	*2.68957*	*1.824992*	*1.82672*
Rad	*0.01*	*0.03*	*0.07*	*0.01*	*0.01*	*0.01*	*0.01*	*0.01*	*0.01*	*0.01*	*0.01*
Ec	*0.001*	*0.001*	*0.001*	*0.003*	*0.005*	*0.001*	*0.001*	*0.001*	*0.001*	*0.001*	*0.001*
Γ	*0.2*	*0.2*	*0.2*	*0.2*	*0.2*	*0.2*	*0.5*	*2*	*-0.2*	*-0.5*	*-2*

The rate of mass transfer (Sh) in all the three quadrants is shown in Tabs 4-6 for different parametric values. It is found that the rate of mass transfer in the lower and upper quadrants decreases with an increase in Ra and that in the middle quadrant it grows with Ra. With respect to the heat source parameter α we find

that the Sherwood number in the middle and upper quadrants grows with an increase in α, while in the lower quadrant it decreases with α (Tab.4). When the molecular buoyancy force dominates over the thermal buoyancy force the rate of mass transfer in the lower and upper quadrants increases, while in the middle quadrant it decreases when the buoyancy forces act in the same direction and for the forces acting in opposite directions the Sherwood number increases in the lower and middle quadrants and decreases in the upper quadrant. With respect to the Schmidt number Sc, we find that the Sherwood number in the lower and upper quadrants increases with Sc≤*1.3* and decreases with higher Sc≥*2.01*, while in the middle quadrant, it decreases with Sc≤*1.3* and increases with Sc≥*2.01*. With reference to S_0, we find that an increase in $S_0>0$ reduces Sh in all the three quadrants, while an increase in $|S_0|$ (*<0*) diminishes Sh in the lower and middle quadrants and increases in the upper quadrant (Tab.5). Table 6 shows that variation of Sh with the radiation parameter N_1, Eckert number Ec and chemical reaction parameter γ. It is found that an increase in N_1 reduces Sh in all the three quadrants. Thus the higher the dissipative heat, the larger the rate of mass transfer in all the three quadrants and for further higher Ec≥*0.05*, the smaller Sh in all the three quadrants. The rate of mass transfer experiences an enhancement in the case of no chemical reaction case, while in the case of a chemical reaction, it is found to grow in the lower and middle quadrants and decreases in the upper quadrant (Tab.6).

Table 4. Sherwood number (Sh) at different levels.

	I	II	III	IV	V
sh1	*-37.949*	*28.5738*	*7.7496*	*-27.99*	*-19.689*
sh2	*0.43571*	*5.77304*	*9.1027*	*0.83571*	*-13.419*
sh3	*38.8204*	*-17.028*	*7.61476*	*48.8204*	*166.73*
Ra	10^2	2×10^2	3×10^2	10^2	10^2
α	*2*	*2*	*2*	*4*	*6*

Table 5. Sherwood number (Sh) at different levels.

	I	II	III	IV	V	VI	VII	VIII	IX	X
sh1	*-37.949*	*-28.176*	*3.09948*	*4.68824*	*-2.0915*	*31.1623*	*12.0954*	*-40.04*	*8.1621*	*3.3357*
sh2	*0.43257*	*2.52872*	*2.5096*	*2.51196*	*19.856*	*9.78076*	*3.68836*	*0.444*	*3.6005*	*3.0479*
sh3	*38.8204*	*33.2336*	*1.91969*	*0.33572*	*10.803*	*-11.601*	*-4.71868*	*41.36*	*-0.961*	*2.7602*
N	*1*	*2*	*-0.5*	*-0.8*	*1*	*1*	*1*	*1*	*1*	*1*
Sc	*1.3*	*1.3*	*1.3*	*1.3*	*0.24*	*0.6*	*2.01*	*1.3*	*1.3*	*1.3*
S0	*0.5*	*0.5*	*0.5*	*0.5*	*0.5*	*0.5*	*0.5*	*1*	*-0.5*	*-1*

Table 6. Sherwood number (Sh) at different levels.

	I	II	III	IV	V	VI	VII	VIII	IX	X	XI
sh1	*12.7969*	*10.6176*	*8.73688*	*28.8124*	*12.988*	*-1.4026*	*-2.94896*	*-3.2822*	*10.1396*	*10.55628*	*10.9834*
sh2	*3.99816*	*3.01012*	*2.45208*	*10.3831*	*4.0639*	*0.34006*	*0.43571*	*-2.986*	*2.57584*	*2.9558*	*3.51308*
sh3	*-4.8006*	*-4.5973*	*-3.8327*	*-8.0463*	*-4.8599*	*2.08272*	*2.2036*	*-2.6897*	*-4.988*	*-4.64464*	*-3.95724*
Rad	*0.01*	*0.03*	*0.05*	*0.01*	*0.01*	*0.01*	*0.01*	*0.01*	*0.01*	*0.01*	*0.01*
Ec	*0.001*	*0.001*	*0.001*	*0.003*	*0.005*	*0.001*	*0.001*	*0.001*	*0.001*	*0.001*	*0.001*
γ	*0.2*	*0.2*	*0.2*	*0.2*	*0.2*	*0.2*	*0.5*	*2*	*-0.2*	*-0.5*	*-2*

Nomenclature

C – concentration
C_p – specific heat at constant pressure
Ec – Eckert number

f_p (p= *1,2,3…..*) – global nodal values
g' – acceleration due to gravity
H – Heaviside function
K – concentration coefficient
K_1 – thermal conductivity
k – permeability of the porous medium
k_{11} – cross diffusivity
Le – Lewis number
N – buoyancy ratio
N_1 – radiation parameter
N_k^i (k= *1,2,3….*) – linear combination of shape function
Nu – Nusselt number
p' – pressure
Q – strength of the heat source
q_r – radiative heat flux
Ra – Rayleigh number
Sc – Schmidt number
Sh – Sherwood number
S_0 – Soret number
T' – temperature
T_c and C_c – temperature and concentration on the cold side walls
T_h and C_h – temperature and concentration on the warm side walls
u' and v' – Darcy velocities along x and y directions
α – heat source parameter
β – thermal expansion of the fluid
β* – volume coefficient
$\theta_1, \theta_2 \ldots \theta_{10}$ – global values of θ
μ – coefficients of viscosity of the fluid
ν – kinematics viscosity of the fluid
ρ′ – density of the fluid
ψ – stream function
$\psi_1, \psi_2 \ldots \psi_{10}$ – global values of ψ
ψ^i, θ^i, C^i – approxiamate values of ψ, θ and C

References

Badruddin I.A., Zainal Z.A., Aswatha N. and Seetharamu K.N. (2006): *Heat transfer in porous cavity under the influence of radiation and viscous dissipation*. – Int. Comm. in Heat and Mass Transfer, vol.33, pp.491-499.

Bankvall C.G. (1972): *Natural convective heat transfer in an insulated structure*. – Lundinst. Tech. Report, vol.38, pp.1-149.

Bankvall C.G. (1973): *Heat transfer in fibrous material*. – J. Test. E; vol.3, pp.235-243.

Bankvall C.G. (1974): *Natural convective in vertical permeable space*. – Warme-and Staffubertragung, vol.7, pp.22-30.

Beckermann C., Ramadhyani S. and Viskanta R. (1987): *Natural convection flow and heat transfer between fluid layer and a porous layer inside a rectangular enclosure*. – Journal of Heat Transfer, vol.109, p.363.

Bejan A. (1979): *On the boundary layer region in a vertical enclosure filled with a porous medium.* – Letters Heat and Mass Transfer. – vol.6, pp.93-102.

Burns P.J., Chow L.C. and Chen S. (1926): Int. J. Heat and Mass Transfer, vol.20, pp.919-926.

Chen B.K.C., Ivey U.M. and Barry J.M. (1970): *Natural convection in enclosed porous medium with rectangular boundaries*. – ASME Journal of Heat Transfer, vol.92, pp.21-27.

Cheng K.S. and Hi J.R. (1987): *Steady, two-dimensional, natural convection in rectangular enclosures with differently heated walls.* – Transaction of the ASME, vol.109, p.400-406.

Chittibabu D., Prasada Rao D.R.V. and Krishna D.V. (2006): *Convection flow through a porous medium in ducts*. – Act Science Indica, vol.30 2M, pp.635-642.

Han-Chien C., Jer-Huan J. and Wei M. (2007): *Mixed convection heat transfer in horizontal rectangular ducts with radiation effects*. –Int. Journal of Heat Mass Transfer, vol.50, pp.2874-2882.

Hickox C.E. and Gartling D.K. (1981): *A numerical study of natural convection in a horizontal porous layer subjected to an end-to-end temperature difference.* – ASME. J. Heat Transfer, vol.103, pp.797-802.

Hiroxhi I., Kazuyoshi N. and Kenjiro S. (2000): *Flow and heat transfer characteristics of backward-facing step laminar flow in a rectangular duct*. – Int. J. Heat and Mass Transfer, vol.43, pp.457-471.

Holst P.H. (1972): *Transient three dimensional natural convection in confined porous media*. – Int. J. Heat Mass Transfer, vol.15, pp.72-89.

Hyun J.M. and Lee J.W. (1990): *Double-diffusive convection in a rectangle with cooperating horizontal gradients of temperature and concentration gradients*. – Int. J. Heat Mass Transfer, vol.33.pp.1605-1617.

Joseph J., Siegel S. and Siegel R. (1964): *Laminar forced convection in rectangular channels with unequal heat addition on adjacent sides*. – Int. J. Heat Mass Transfer, vol.71, pp.733-741.

Kakutani J. (1958): *Effect of transverse magnetic field on the flow due to an oscillatinf flat plate.* – J. Phys. Soc., Japan, vol.13, p.1504-1509.

Kamotani, Wang L.W., Ostrach S. and Jiang H.D. (1985): *Experimental study of natural convection in shallow enclosures with horizontal temperature and concentration gradients*. – Int. J. Heat Mass Transfer, vol.28, pp.165-173.

Kermant B.C.C: *Natural convection flow and heat transfer between a fluid layer and a porous layer inside a rectangular enclosure*. – Heat Transfer Laboratory, Purdue, University, Indiana.

Lauriant F. (1984): *Natural convection and radiation on enclosure partially, filled with a porous insulation.* – ASME, pp.84-107.

Lee L., Hyun M.T. and Kim K.W. (1985): *Natural convection in confined fluids with combined horizontal temperature and concentration gradients*. – Int. J. Heat Mass Transfer, vol.31, pp.1969-1977.

Lee L.W. and Hyun J.M. (1990): *Double-diffusive convection in a rectangle with opposing horizontal and concentration 8 gradients*. – Int. J. Heat and Mass Transfer, vol.33, pp.1619-1632.

Morrison F.A. (1973): *Transient multiphase multi component flow in porous media*. – Int. J. Heat Mass Transfer, vol.16, pp.2331-2341.

Ostrach S., Jiang H.D. and Kamotani Y. (1987): *Thermo solutal convection in shallow enclosures*. – ASME – JSME Thermal Engineering Joint Conference, Hawali.

Padmalatha K. (1997): *Ph.D. Thesis on "Finite element analysis of laminar convection flow through a porous medium in ducts,"* S.K. University, Anantapur, (A. P) India.

Padmavathi A. (2009): *Finite element analysis of the convective heat transfer flow of a viscous in compressible fluid in a rectangular duct with radiation, viscous dissipation with constant heat source*. – Jour. Phys. and Appl. Phys., vol.2.

Poulikakos D. and Bejan A. (1983): *Natural convection in vertically and horizontally layered porous media heated from side*. – Int. J. Heat and Mass Transfer, vol.26, pp.1805-1813.

Prasad V. and Kulacki F.A. (1984): *Convective heat transfer in a rectangular porous cavity effect of aspect ratio flow structure and heat transfer*. – ASME Journal of Heat Transfer, vol.106, pp.158-165.

Prasad V. and Kulacki F.A. (1984): *Natural convection in a vertical porous annulus*. – Int. J. Heat Mass Transfer, vol.27, pp.207-219.

Ranga Reddy M. (1997): *Heat and mass transfer by natural convection through a porous medium in ducts*. – Ph. D thesis, S.K. University, Anantapur.

Reddaiah P. (2010): *Heat and mass transfer flow of a viscous fluid in a duct of rectangular cross section by using finite element analysis*. – European J. of Prime and Applied Mathematics (Accepted).

Revnic C., Grosan J., Pop T. and Ingham D.B. (2011): *Magnetic field effect on the unsteady free convection flow in a square cavity filled with a porous medium with a constant heat generation*. – Int. J. Heat and Mass Transfer, vol.54, pp.1734-1742.

Ribando R.J. and Torrance K.E. (1976): *Natural convection in a porous medium effects of confinement, variable permeability and thermal boundary conditions, trans*. – Am. Soc. Mech. Engrs. Series. C.J. Heat Transfer, vol.98, pp.42-48.

Rubin A. and Schweitzer S. (1972): *Heat transfer in porous media with phase change*. – Int. J. Heat Mass Transfer, vol.15, pp.43-59.

Saffman P.G. (1969): Studies in Applied Mathematics, vol.50, p.537.

San J. (1984): *Natural convection in a rectangular porous cavity with constant heat flux as vertical wall*. – Trans. of ASME, vol.106, p.252.

Seki N., Fukusako S. and Inaba H. (1981): *Heat transfer in a confined rectangular cavity packed with porous media*. – Int. J. of Heat and Mass Transfer, vol.21, pp.985-989.

Sivaiah S. (2004): *Thermo-diffusion effects on convective heat and mass transfer through a porous medium in ducts*. – Ph. D Thesis, S.K. University, Anantapur, India.

Tamony B., Krishna P.P.V., Roy S. and Pop I. (2011): *Finite element based heat line approach to study mixed convection in a porous square cavity with various wall thermal boundary conditions*. – Int. J. Heat and Mass Transfer, vol.54, pp.1706-1727.

Teoman A., Hayati O. and Betel A. (1998): *Heat transfer and flow structure in a rectangular channel with wing -1. Type vortex Generator*. – Tr. J. of Engineering and Environmental Science, vol.22, pp.185-195.

Tien C.L. and Hong J.T. (1985): *Natural convection in porous media under non-darcian and non-uniform permeability convections.* – In: Natural convection (S. Kakac, et. al. Eds.), Washington, D.C, Hemisphere.

Trevisan O.V. and Bejan A. (1986): *Mass and heat transfer by natural convection in a vertical slot filled with porous medium*. – Int. J. Heat Mass Transfer, vol.29, pp.403-415.

Trevisan O.V. and Bejan A. (1987): *Combined heat and mass transfer by natural convection in a vertical enclosure*. – ASME, J. Heat Transfer, vol.109, pp.104-112.

Turner B.C. and Flack R.D. (1980): *The experimental measurement of natural convective heat transfer in rectangular enclosures with concentrated energy source*. – Trans. of ASME, vol.102, pp, 236-242.

Verschoor J.D. and Greebler P. (1952): *Heat transfer by gas conduction and radiation in fibrous insulation*. – Trans. Am. Soc. Mech. Engrs, pp.961-968.

Viskanta R., Bergman T.L. and Incropera F.P. (1985): *Double differential natural convection.* – In: Natural convection fundamentals and applications (S. Kakac, W. Aung and R. Viskanta, Eds.). – Washington, D.C., Hemisphere, pp.1075-1099.

Received: November 27, 2012

Revised: June 17, 2013

Appendix

$$a_{12} = -\frac{20}{3s} - \frac{6\,ASP\alpha}{s} - \frac{2P\lambda}{5} + \frac{4P\,f_{2}}{15} - \frac{4}{15}P\alpha\,g_{2} + \frac{8\,ASP\alpha\,h_{2}}{s} - \frac{2\,ASP\alpha\,h_{3}}{s},$$

$$a_{13} = \frac{10}{3s} + \frac{ASP\alpha}{s} + \frac{P\lambda}{15} - \frac{P\,f_{2}}{15} - \frac{P\,f_{3}}{30} + \frac{1}{15}P\alpha\,g_{2} + \frac{1}{30}P\alpha\,g_{3} - \frac{4\,ASP\alpha\,h_{2}}{3s} + \frac{ASP\alpha\,h_{3}}{3s},$$

$$a_{22} = \frac{4\left(-100 + Ps\left(-\lambda - f_3 + \alpha g_3\right)\right)}{15s},$$

$$a_{23} = \frac{200 + Ps\left(\lambda + 8f_2 + 3f_3 + \alpha\left(-8g_2 - 3g_3 - \frac{5AS\left(-3s + 4sh_2 - sh_3\right)}{s^2}\right)\right)}{15s},$$

$$a_{32} = -\frac{20}{3s} - \frac{4Pf_2}{15} - \frac{2Pf_3}{5} + \frac{4}{15}P\alpha g_2 + \frac{2}{5}P\alpha g_3,$$

$$a_{33} = \frac{20}{3s} + \frac{ASP\alpha}{2s} + \frac{P\lambda}{30} + \frac{Pf_2}{5} - \frac{Pf_4}{5} + \frac{Pf_5}{30} - \frac{1}{5}P\alpha g_2 + \frac{1}{5}P\alpha g_4 - \frac{1}{30}P\alpha g_5 - \frac{2ASP\alpha h_2}{3s} + \frac{ASP\alpha h_3}{6s},$$

$$a_{43} = \frac{200 + Ps\left(-3f_3 - 8f_4 + f_5 + 3\alpha g_3 + 8\alpha g_4 - \alpha g_5\right)}{15s},$$

$$a_{53} = \frac{10}{3s} + \frac{Pf_3}{30} + \frac{Pf_4}{15} + \frac{Pf_5}{15} - \frac{1}{30}P\alpha g_3 - \frac{1}{15}P\alpha g_4 - \frac{1}{15}P\alpha g_5,$$

$$a_{34} = -\frac{20}{3s} + \frac{2Pf_3}{5} + \frac{4Pf_4}{15} - \frac{2}{5}P\alpha g_3 - \frac{4}{15}P\alpha g_4, \qquad a_{44} = \frac{4\left(-100 + Ps\left(f_3 - f_5 - \alpha g_3 + \alpha g_5\right)\right)}{15s},$$

$$a_{54} = -\frac{20}{3s} - \frac{4Pf_4}{15} - \frac{2Pf_5}{5} + \frac{4}{15}P\alpha g_4 + \frac{2}{5}P\alpha g_5,$$

$$a_{35} = \frac{10}{3s} - \frac{Pf_3}{15} - \frac{Pf_4}{15} - \frac{Pf_3}{30} + \frac{1}{15}P\alpha g_3 + \frac{1}{15}P\alpha g_4 + \frac{1}{30}P\alpha g_5,$$

$$a_{45} = \frac{200 + Ps\left(-f_3 + 8f_4 + 3f_5 + \alpha\left(g_3 - 8g_4 - 3g_5\right)\right)}{15s},$$

$$a_{55} = \frac{20}{3s} - \frac{Pf_3}{30} + \frac{Pf_4}{5} - \frac{Pf_6}{5} + \frac{Pf_7}{30} + \frac{1}{30}P\alpha g_3 - \frac{1}{5}P\alpha g_4 + \frac{1}{5}P\alpha g_6 - \frac{1}{30}P\alpha g_7,$$

$$a_{65} = \frac{200 + Ps\left(-3f_5 - 8f_6 + f_7 + 3\alpha g_5 + 8\alpha g_6 - \alpha g_7\right)}{15s},$$

$$a_{75} = \frac{10}{3s} + \frac{P f_5}{30} + \frac{P f_6}{15} + \frac{P f_7}{15} - \frac{1}{30} P\alpha g_5 - \frac{1}{15} P\alpha g_6 - \frac{1}{15} P\alpha g_7,$$

$$a_{56} = -\frac{20}{3s} + \frac{2P f_5}{5} + \frac{4P f_6}{15} - \frac{2}{5} P\alpha g_5 - \frac{4}{15} P\alpha g_6, \qquad a_{66} = \frac{4\left(-100 + Ps\left(f_5 - f_7 - \alpha g_5 + \alpha g_7\right)\right)}{15s},$$

$$a_{76} = -\frac{20}{3s} - \frac{4P f_6}{15} - \frac{2P f_7}{5} + \frac{4}{15} P\alpha g_6 + \frac{2}{5} P\alpha g_7,$$

$$a_{57} = \frac{10}{3s} - \frac{P f_5}{15} - \frac{P f_6}{15} - \frac{P f_7}{30} + \frac{1}{15} P\alpha g_5 + \frac{1}{15} + P\alpha g_6 + \frac{1}{30} P\alpha g_7,$$

$$a_{67} = \frac{200 + Ps\left(-f_5 + 8 f_6 + 3 f_7 + \alpha\left(g_5 - 8 g_6 - 3 g_7\right)\right)}{15s},$$

$$a_{77} = \frac{20}{3s} - \frac{P f_5}{30} + \frac{P f_6}{5} - \frac{P f_8}{5} + \frac{P f_9}{30} + \frac{1}{30} P\alpha g_5 - \frac{1}{5} P\alpha g_6 + \frac{1}{5} P\alpha g_8 - \frac{1}{30} P\alpha g_9,$$

$$a_{87} = \frac{200 + Ps\left(-3 f_7 - 8 f_8 + f_9 + 3\alpha g_7 + 8\alpha g_8 - \alpha g_9\right)}{15s},$$

$$a_{97} = \frac{10}{3s} + \frac{P f_7}{30} + \frac{P f_8}{15} + \frac{P f_9}{15} - \frac{1}{30} P\alpha g_7 - \frac{1}{15} P\alpha g_8 - \frac{1}{15} P\alpha g_9,$$

$$a_{78} = -\frac{20}{3s} + \frac{2P f_7}{5} + \frac{4P f_8}{15} - \frac{2}{5} P\alpha g_7 - \frac{4}{15} P\alpha g_8, \qquad a_{88} = \frac{4\left(-100 + Ps\left(f_7 - f_9 - \alpha g_7 + \alpha g_9\right)\right)}{15s},$$

$$a_{98} = -\frac{20}{3s} - \frac{4P f_8}{15} - \frac{2P f_9}{5} + \frac{4}{15} P\alpha g_8 + \frac{2}{5} P\alpha g_9,$$

$$a_{79} = \frac{10}{3s} - \frac{P f_7}{15} - \frac{P f_8}{15} - \frac{P f_9}{30} + \frac{1}{15} P\alpha g_7 + \frac{1}{15} P\alpha g_8 + \frac{1}{30} P\alpha g_9,$$

$$a_{89} = \frac{200 + Ps\left(-f_7 + 8 f_8 + 3 f_9 + \alpha\left(g_7 - 8 g_8 - 3 g_9\right)\right)}{15s},$$

$$a_{99} = \frac{20}{3s} - \frac{P f_{7}}{30} + \frac{P f_{8}}{5} - \frac{P f_{10}}{5} + \frac{P f_{11}}{30} + \frac{1}{30} P\alpha g_{7} - \frac{1}{5} P\alpha g_{8} + \frac{1}{5} P\alpha g_{10},$$

$$a_{109} = \frac{200 + Ps\left(-3 f_{9} - 8 f_{10} + f_{11} + 3\alpha g_{9} + 8\alpha g_{10} \right)}{15s},$$

$$a_{119} = \frac{10}{3s} + \frac{P f_{9}}{30} + \frac{P f_{10}}{15} + \frac{P f_{11}}{15} - \frac{1}{30} P\alpha g_{9} - \frac{1}{15} P\alpha g_{10},$$

$$a_{910} = -\frac{20}{3s} + \frac{2P f_{9}}{5} + \frac{4P f_{10}}{15} - \frac{2}{5} P\alpha g_{9} - \frac{4}{15} P\alpha g_{10},$$

$$a_{1010} = \frac{4\left(-100 + Ps\left(f_{9} - f_{11} - \alpha g_{9} \right) \right)}{15s}, \qquad a_{1110} = -\frac{20}{3s} - \frac{4P f_{10}}{15} - \frac{2P f_{11}}{5} + \frac{4}{15} P\alpha g_{10},$$

$$b_{1,2} = -\frac{2}{3} - \frac{40}{3s}, \qquad b_{1,3} = \frac{1}{6} + \frac{5}{3s}, \qquad b_{2,2} = \frac{8}{3} + \frac{80}{3s}, \qquad b_{2,3} = -2 - \frac{40}{3s},$$

$$b_{3,2} = -2 - \frac{40}{3s}, \qquad b_{3,3} = \frac{14}{3} + \frac{70}{3s}, \qquad b_{3,4} = -\frac{10}{3} - \frac{40}{3s}, \qquad b_{3,5} = \frac{1}{2} + \frac{5}{3s},$$

$$b_{4,3} = -\frac{10}{3} - \frac{40}{3s}, \qquad b_{4,4} = 8 + \frac{80}{3s}, \qquad b_{4,5} = -\frac{14}{3} - \frac{40}{3s}, \qquad b_{5,3} = \frac{1}{2} + \frac{5}{3s},$$

$$b_{5,4} = -\frac{14}{3} - \frac{40}{3s}, \qquad b_{5,5} = \frac{28}{3} + \frac{70}{3s}, \qquad b_{5,6} = -6 - \frac{40}{3s}, \qquad b_{5,7} = \frac{5}{6} + \frac{5}{3s},$$

$$b_{5,5} = -6 - \frac{40}{3s}, \qquad b_{5,6} = \frac{40}{3} + \frac{80}{3s}, \qquad b_{5,7} = -\frac{22}{3} - \frac{40}{3s}, \qquad b_{7,5} = \frac{5}{6} + \frac{5}{3s},$$

$$b_{7,6} = -\frac{22}{3} - \frac{40}{3s}, \qquad b_{7,7} = 14 + \frac{70}{3s}, \qquad b_{7,8} = -\frac{26}{3} - \frac{40}{3s}, \qquad b_{7,9} = \frac{7}{6} + \frac{5}{3s},$$

$$b_{8,7} = -\frac{26}{3} - \frac{40}{3s}, \qquad b_{8,8} = \frac{56}{3} + \frac{80}{3s}, \qquad b_{8,9} = -10 - \frac{40}{3s}, \qquad b_{9,7} = \frac{7}{6} + \frac{5}{3s},$$

$$b_{9,8} = -10 - \frac{40}{3s}, \qquad b_{9,9} = \frac{56}{3} + \frac{70}{3s}, \qquad b_{9,10} = -\frac{34}{3} - \frac{40}{3s}, \qquad b_{10,9} = -\frac{34}{3} - \frac{40}{3s},$$

$$b_{10,10} = 24 + \frac{80}{3s}, \qquad b_{11,9} = \frac{3}{2} + \frac{5}{3s}, \qquad b_{11,10} = -\frac{38}{3} - \frac{40}{3s}, \qquad b_{11,11} = -1 - s.$$